Biosensors and Bioelectronics 250 (2024) 116050

Contents lists available at ScienceDirect

Biosensors and Bioelectronics

journal homepage: www.elsevier.com/locate/bios

2D graphene-based advanced nanoarchitectonics for electrochemical biosensors: Applications in cancer biomarker detection

Soumajit Mukherjee [a,1], Atripan Mukherjee [a,b,1], Zuzana Bytesnikova [a], Amir M. Ashrafi [a], Lukas Richtera [a,c], Vojtech Adam [a,*]

[a] Department of Chemistry and Biochemistry, Mendel University in Brno, Zemedelska 1, CZ-613 00, Brno, Czech Republic
[b] ELI Beamlines Facility, The Extreme Light Infrastructure ERIC, Za Radnici 835, 252 41, Dolni Breznany, Czech Republic
[c] Central European Institute of Technology, Brno University of Technology, Purkynova 123, CZ-612 00, Brno, Czech Republic

ARTICLE INFO

Keywords:
2D nanocomposites
Sensor development
Electrochemical biosensor
Cancer biomarker
Graphene

ABSTRACT

Low-cost, rapid, and easy-to-use biosensors for various cancer biomarkers are of utmost importance in detecting cancer biomarkers for early-stage metastasis control and efficient diagnosis. The molecular complexity of cancer biomarkers is overwhelming, thus, the repeatability and reproducibility of measurements by biosensors are critical factors. Electrochemical biosensors are attractive alternatives in cancer diagnosis due to their low cost, simple operation, and promising analytical figures of merit. Recently graphene-derived nanostructures have been used extensively for the fabrication of electrochemical biosensors because of their unique physicochemical properties, including the high electrical conductivity, adsorption capacity, low cost and ease of mass production, presence of oxygen-containing functional groups that facilitate the bioreceptor immobilization, increased flexibility and mechanical strength, low cellular toxicity. Indeed, these properties make them advantageous compared to other alternatives. However, some drawbacks must be overcome to extend their use, such as poor and uncontrollable deposition on the substrate due to the low dispersity of some graphene materials and irreproducibility of the results because of the differences in various batches of the produced graphene materials. This review has documented the most recently developed strategies for electrochemical sensor fabrication. It differs in the categorization method compared to published works to draw greater attention to the wide opportunities of graphene nanomaterials for biological applications. Limitations and future scopes are discussed to advance the integration of novel technologies such as artificial intelligence, the internet of medical things, and triboelectric nanogenerators to eventually increase efficacy and efficiency.

1. Introduction

A biomolecule, referred to as a biomarker, is a quantifiable indicator of a pathophysiological event in the biological sample that can be related to an emergent or progressing disease. Regular monitoring of the presence or the level of a biomarker in the body fluid or tissue is an excellent approach to predicting and detecting diseases to aid prognosis and treatment plans. Biomarker detection has been extensively explored for diagnosing cardiovascular and neurological diseases, pathogenic infections, immunological and genetic disorders, and cancer (Henry and Hayes, 2012; Chatterjee and Zetter, 2005; Pavanello and Clonfero, 2000). A wide range of molecular biomarkers have been established for early and rapid diagnosis of cancer, and their roles in different cancer types have been explored over the years (Fig. 1). Those include DNA/RNA (Isbell et al., 2018), biological macromolecules such as proteins (Rifai et al., 2006; Ordonez, 2014), noncoding RNAs (Li et al., 2017; Cuk et al., 2013; Mitchell et al., 2008), chemical metabolites (Wu et al., 2004; Monteiro et al., 2017), or circulating tumor cells in biological fluids (Lai et al., 2017; Chen et al., 2016). Alongside detecting an ongoing carcinoma, biomarkers have helped predict the onset of tumors based on health conditions, genetic mutations, and family history.

The traditional and advanced methods employed for the detection of cancer biomarkers in clinical diagnosis include a variety of blood tests, biopsy, CT scan, the enzyme-linked immunosorbent assay (ELISA), quantitative polymerase chain reaction (PCR), and next-generation sequencing (NGS). Although these methods provide precise and

* Corresponding author.
E-mail address: vojtech.adam@mendelu.cz (V. Adam).
[1] Equal contribution.

https://doi.org/10.1016/j.bios.2024.116050
Received 15 September 2023; Received in revised form 1 January 2024; Accepted 17 January 2024
Available online 24 January 2024

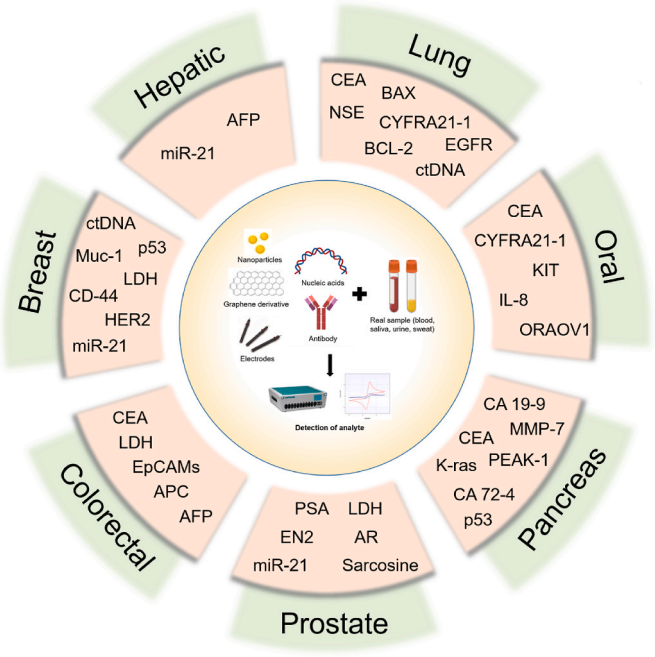

Fig. 1. Transducer materials for the fabrication of electrochemical biosensors and established prognostic biomarkers for different cancer types (abbreviations are listed at the end of this review).

accurate detection, each one suffers from the inherent drawbacks, which overall can be summarized as false-positive or false-negative results due to the interferences, the high cost of reagents and equipment, risk of contamination during the sample preparation, long turnaround time, and requirement of skilled people in running the experiments and data analysis. Electrochemical biosensors, due to their intrinsic features that include simplicity, cost-effectiveness, and small dimensions, can potentially advance the diagnosis, and consequently the survival rate in cancer therapy. An ideal user-friendly point-of-care (PoC) biosensor would be affordable and able to detect biomarkers rapidly from a small volume of the fluid sample with minimal labor and high specificity, enabling PoC by the patient. Indeed, the abovementioned benefits necessitate greater investment in the development of electrochemical sensory devices alongside conventional diagnosis methods. The biomedical field has witnessed a surging rise in the application of low-cost nanomaterials in imaging and drug delivery owing to their small size, and excellent physiochemical properties. Studies have established the effective use of gold and silver nanoparticles (NPs) and carbon-based nanomaterials such as nanotubes, graphene, and graphene oxide (GO) in the development of smart biosensors, cancer treatment, and tissue engineering (Tauro et al., 2012; Kim et al., 2011; Chen et al., 2012; Zhang et al. 2010, 2011; Siemer et al., 2020). Graphene is a carbon-based nanomaterial that exhibits remarkable thermal, electrical, and mechanical properties. In recent years, graphene-based nanomaterials have been increasingly utilized as platforms for modification and increased stability in nano-engineering, such as to support artificial photosynthesis (Yang et al., 2014), to enhance and optimize the photocatalytic performance of semiconductors (Han et al., 2016; Yang et al., 2015; Gogoi et al., 2021), for CO_2 reduction from the environment (Lu et al., 2020), to enhance hydrogen evolution activity (Li et al., 2018), and to facilitate oxidation of aromatic alcohols in water media (Bellardita et al., 2018) etc. Graphene derivatives, such as GO and its reduced form rGO, are advantageous for the development of biosensors due to their large surface area, superior electrical conductivity, and excellent biocompatibility (Kim et al., 2017; Geim and Novoselov, 2007). The graphene derivatives edge out other contemporary nanomaterials for detecting the different cancer biomarkers, which are presented as a comparison in Table 1. The parameters such as ease of synthesis, immobilization strategy used, biocompatibility, recyclability, and response time were considered significant factors in a critical comparison. Other alternatives include metal nanoparticles, metal-organic frameworks, conductive polymers, and carbon nanotubes (CNTs). The nanomaterials enhance the surface area due to surface to surface-to-air-to-volume ratio, and the good diffusion rate between the electrolyte and the electrode. Despite signal amplification properties, they tend to undergo agglomeration as a primary drawback to act as nanocatalysts, thereby losing the surface area for bioreceptor immobilization (Holzinger et al., 2014). The intrinsic property of CNTs favors large surface area, and electrical conductivity and can form nanocomposites by electrochemically synthesized Au NPs. Though CNTs and graphene share similar properties, graphene has clear advantages, as it is cheap to produce and does not have metallic impurities like CNTs (Yang et al., 2010). The 2D plane of graphene can be functionalized easily with functional groups, which ultimately helps bioreceptor immobilization, a key criterion in biosensor fabrication. The high electron mobility makes it promising in electrochemical biosensors. For the fabrication of biosensors, transducer materials are incorporated into a sensing platform to amplify the signal upon the detection of an analyte using electrochemical techniques (Fig. 1).

The biocompatibility and surface area of graphene derivatives stabilize and enhance the immobilization of bio-recognition elements to boost the sensitivity of detection. This review aims to discuss various strategies to prepare graphene and its different nanocomposite-based electrochemical biosensors for the selective detection of different types of cancer biomarkers. In comparison to contemporary published studies (Balaji and Zhang, 2017; Janegitz et al., 2017; Peña-Bahamonde et al., 2018; Xu et al., 2019; Iannazzo et al., 2021), where various strategies for the fabrication of biosensors have been categorized based on electrochemical techniques or analyte type, the following chapters in this review are categorized based on the detection of different biomarkers clinically correlated to different cancer types. It is beneficial to propose a holistic view of the usability of graphene derivatives in the detection of a wide range of cancers and other clinical conditions. Fig. 1 presents different types of cancers and corresponding biomarkers that

Table 1
Advantages of graphene-based nanomaterials over other carbon nanomaterials for the fabrication of electrochemical biosensor.

Other alternatives	Ease of synthesis	Immobilization strategy	Dispersion	Stability	Cost	Electrical Conductivity	Ref.
Metal oxide nanoparticle, metal nanoparticles	Electrochemical synthesis, Hydrothermal	Covalent bonding, adsorption, cross-linking	Bi_2O_3, AuNPs, PtNPs	Low as NPs can agglomerate	Medium	Medium	(Kou et al., 2016; Palomar et al., 2020)
Conductive polymer	Electrochemical, chemical synthesis	Covalent	Dopamine, polypyrrole	Good as the deposition is controlled	High	High	(Palomar et al., 2020; Wang et al., 2017)
Metal-organic framework	Hydrothermal, solvothermal, microwave, electrochemical	Covalent, Non-covalent, Cross-linking agent	Cu-MOF	High	Medium	High	(Fu et al., 2023; Liang et al., 2019)
Carbon nanotubes	Thermal CVD method	Cross-linker	MWCNTs, DWCNTs	Medium	Low	High	Wang et al. (2017)

are discussed in this review. Different biosensors developed for cancer biomarkers were critically compared in terms of the analytical figures of merit. More importantly, the related challenges and ideation are discussed from a future perspective.

2. Physiochemical properties of graphene-based nanomaterials

Graphene and its derivatives have been applied for sensor fabrication due to their unique physiochemical properties (Park and Ruoff, 2009). They are 2D nanomaterials, theoretically a single layer having one dimension in the nanoscale (Geim and Novoselov, 2007). Graphene is composed of only a single sheet of carbon atoms and appears in a honeycomb lattice where the sheet dimension varies from nanometers to centimeters in different layers (Soldano et al., 2010). The presence of carbon atoms in the sp^2 hybridization state enables electrons to populate a π–π conjugation system, which enables the free movement of electrons and makes the material excellent for electron transfer (Park and Ruoff, 2009). Material to be called graphene should consist of exactly one layer of carbon atoms, whether in case of multiple layers of carbon atoms stacked together, it would be considered as multilayer graphene or graphite, depending on the number of layers and their arrangement. The number of graphene layers has a significant impact on its utilization in electrochemistry (Bonanni et al., 2012). However, in electrochemical applications, multilayer graphene materials such as graphene films or graphene foams are often preferred. Single-layer graphene exhibits extremely high conductivity, whereas when multiple layers are stacked, a slight reduction in conductivity can be observed (Castelletto and Boretti, 2021). Multi-layer graphene materials have a larger surface area compared to single-layer graphene (Murata et al., 2019) and the surface area of the former is proportional to the number of layers it has. This allows for better adsorption and interaction with electrochemically active species, thereby enhancing their electrochemical performance (Goh and Pumera, 2010). Multi-layer graphene materials are generally cheaper for production and more readily available than single-layer graphene. This makes them a more practical and economically viable choice for many electrochemical applications (Castelletto and Boretti, 2021). Graphene is not always completely free of heteroatoms, especially under atmospheric conditions and in the presence of defects and edges. Heteroatoms, such as oxygen, nitrogen, or hydrogen, can be introduced during the synthesis, transfer, or handling of graphene (Hofer et al., 2019). Graphene prepared through various methods, including chemical vapor deposition (CVD) or mechanical exfoliation, typically contains impurities or adsorbed molecules from the surrounding environment (Ambrosi and Pumera, 2014). These impurities can include water molecules (humidity), oxygen, or other atmospheric gases that can adsorb onto the graphene surface or interact with defects and edges. Furthermore, during the synthesis or processing of graphene, defects and edges can naturally occur. These defects can involve the disruption of the carbon lattice, vacancies, or the presence of grain boundaries. Defects and edges provide reactive sites where heteroatoms can be absorbed or chemically bound. Therefore, it is common for graphene to have some level of heteroatoms, adsorbates, or defects, especially under ambient conditions (Carraro et al., 2022).

Unlike the graphene definition, GO includes oxygen-containing functional groups on its surface. It has been reported that GO exhibits carboxyl, hydroxyl, and epoxy functional groups on the edges and basal plane (Geim and Novoselov, 2010). The present functional groups on the GO surface are open to one-step decoration with nanoparticles with simultaneous reduction (Durovic et al., 2022). rGO is synthesized by chemical, electrochemical, biological, photochemical, or thermal methods to remove oxygen-containing functional groups from GO and hence possesses high thermal conductivity, mechanical durability, and an enhanced electron transfer rate with a higher surface area (Agarwal and Zetterlund, 2021). rGO is often considered an intermediate state between graphene and GO, with reduced oxygen content compared to GO but not as pristine as pure graphene. rGO exhibits properties that are distinct from both graphene and GO. It retains some of the electrical conductivity of graphene while also maintaining certain functional characteristics associated with the remaining oxygen groups. The presence of functional groups on rGO provides reactive sites that can be utilized for the binding or anchoring of various nanoparticles or other functional materials. These functional groups, such as hydroxyl, epoxy, or carboxyl groups, can serve as attachment points for chemical interactions. The binding of nanoparticles to rGO can lead to the formation of graphene-based nanocomposites with enhanced properties or new functionalities. For example, the incorporation of metal nanoparticles onto rGO can result in enhanced catalytic activity, while the integration of semiconductor nanoparticles can give rise to improved optical or electronic properties. The choice of nanoparticles and the specific functional groups on rGO can be tailored to achieve desired properties or functionalities in the resulting nanocomposite.

Carbon allotropes, in general, offer significant advantages in increasing the specific surface area of the electrode, as a larger surface area typically promotes enhanced electron transfer. The average surface area of rGO is 110.16 $m^2\ g^{-1}$ (Paranthaman et al., 2018) while monolayer graphene has an average surface area as high as 2600 $m^2\ g^{-1}$ (Guo et al., 2014). Young's modulus is a property of the material that entails how easily it can stretch and deform and is defined as the ratio of tensile stress to tensile strain. Young's modulus of flat sheet-like graphene is approximately 1.0 TPa (Lee et al., 2008; Papageorgiou et al., 2017), whereas Young's modulus of wrinkled graphene is around 250 GPa (Gomez-Navarro et al., 2008). The Young's modulus of the monolayer GO sheets was calculated experimentally to be in the order of 250 GPa. The Young's modulus of reduced graphene oxide (rGO) can vary depending on factors such as the specific reduction method, and the degree of reduction (Teklu et al., 2019). Generally, the mechanical strength of rGO is diminished compared to graphene due to the presence of defects and residual oxygen (Gomez-Navarro et al., 2008). Graphene demonstrates favorable values of essential parameters critical for its application in biosensor fabrication. However, while rGO exhibits lower conductivity compared to both single-layer and multilayer graphene (as shown in Table 2), its surface's ease of decoration and the potential to confer desired properties to nanocomposites can complicate the decision of which 2D material is more suitable for biosensor fabrication.

Table 2
Preparation methods and conductivity of 2D graphene-based nanomaterials.

Graphene	Chemical vapor deposition on Cu	Thickness ~2 nm	≈1.6 × 105 S cm^{-1}	Pei & Cheng (2012)
	Layer exchange technique on Ni	multilayer	≈2700 S cm^{-1}	Murata et al. (2019)
rGO	Thermal reduction (annealing)	300 °C	≈2.3 S cm^{-1}	Lim et al. (2021)
		600 °C	≈14.6 S cm^{-1}	Lim et al. (2021)
		900 °C	≈380 S cm^{-1}	Wang et al. (2008)
		1000 °C	≈550 S cm^{-1}	Wang et al. (2008)
		2000 °C	≈2000 S cm^{-1}	Wu et al. (2009)
	Chemical reduction	Hydrazine	≈99.69 S cm^{-1}	Fernandez-Merino et al. (2010)
		Sodium borohydride	≈16.6 S cm^{-1}	Dreyer et al. (2010)
		Ascorbic acid	≈77 S cm^{-1}.	Fernandez-Merino et al. (2010)
		Mixture of hydroiodic acid with acetic acid	≈304 S cm^{-1}	Shao et al. (2010)
		Hydroiodic acid (55 %)	≈298 S cm^{-1}	Pei et al. (2010)

Table 3
Developed electrochemical biosensors for the detection of oral cancer biomarkers.

Analyte	EC techniques	Fabrication	LOD	Sensitivity	Range of detection	Ref.
CYFRA21-1	CV, DPV, EIS	BSA/anti-CYFRA21-1/APTES/ZrO_2–RGO/ITO	122 pg mL^{-1}	3.00 μA mL ng^{-1} cm^{-2}	2.00–22.0 ng mL^{-1}	Kumar et al. (2016)
CYFRA21-1	CV, EIS	BSA/anti-CYFRA21-1/APTES/nY_2O_3/ITO	10.0 pg mL^{-1}	904 Ω mL ng^{-1} cm^{-2}	10.0 pg mL^{-1} – 50.0 ng mL^{-1}	Kumar et al. (2019)
CYFRA21-1	CV, EIS, DPV	BSA/anti-CYFRA21-1/ncCeO_2–rGO/ITO	625 fg mL^{-1}	14.5 μA mL ng^{-1} cm^{-2}	625 fg mL^{-1} – 15.0 ng mL^{-1}	Pachauri et al. (2018)
IL-8	CV, EIS, DPV	IL8/anti-IL8/Au NPs-rGO/ITO	72.7 pg mL^{-1}	29.0 nA mL pg^{-1} cm^{-2}	500 fg mL^{-1} – 4.00 ng mL^{-1}	Verma et al. (2017)
ORAOV1	CV, PEC	Ag NCs/T7 Exo- H1-(H2-2)-Au NPs/MCH/Track/ H_2PtCl_6-He-GO/GCE	0.330 fmol mL^{-1}	0.38 μA log nmol L^{-1} cm^{-2}	15.0 fmol mL^{-1} – 1.50 nmol mL^{-1}	Mo et al. (2020)

3. Immobilization of graphene derivatives on biosensor platform

Bioreceptor immobilization onto the graphene derivatives is vital for fabricating biosensors for cancer biomarker detection. The large surface area of graphene-based nanomaterials acts as a supporting matrix for immobilizing enzymes, antibodies, proteins, and nucleic acids (DNA and RNA) that act as recognizing modules. The presence of various functional surface groups such as hydroxyl, carboxylic, and epoxides on the surface of the GO acts as anchors for the immobilized biomolecules. Different strategies were applied to incorporate bioreceptors on the GO surface by exploiting the presence of modifiable surface groups by entrapment, cross-linking, covalent modifications, and weak interactions (Pattammattel et al., 2013). Therefore, immobilization on the GO can be efficiently done as it allows targeted adsorption of the bioreceptor without affecting its activity or conformation (Yang et al., 2017).

Affinity immobilization is a controlled way and limits the chances of nonspecific adsorptions of bioreceptors on the surface of the GO impacting an effective orientation or structure of the receptors. Chitosan (Hou et al., 2016), dialdehyde starch (Chen et al., 2018), and dopamine (Zhang et al., 2012) act as flexible chains to link the biological macromolecules for support, thereby marginalizing the collision between the electrochemically active enzyme and supporting matrix to maintain the correct enzyme conformation. GO has been reportedly modified with polyethylene glycol (PEG) (Jin et al., 2012), N-hydroxy succinimide ester (Alava et al., 2013), ε-poly-L-lysine (Wu et al., 2015), polyethyleneimine (Xia et al., 2016), and glycans (Hernandez-Cancel et al., 2015) and have been used to improve bioreceptor stabilization. Hydrophilic polymers provide controllable chain lengths with significant biocompatible properties. The modification of GO with PEG-NH_2 offered amine groups on the surface resulting in neutralization of the negative charge leading to favorable adsorption of proteins, enhancing solubility, and thereby reducing the nanomaterial aggregation. The non-covalent treatments like van der Waals interactions, hydrophobic interaction, electrostatic forces, and π-π stacking enhance interactions, biocompatibility, and solubility (Yang et al., 2013). For instance, robust hydrophilic coupling of PEG-grafted poly (maleic anhydride-alt-1-octadecene) was used to modify the rGO surface to form an alkyl terminal group for modification (Yang et al., 2012). Cholesterol hyaluronic acid (Miao et al., 2013), polyoxyethylene sorbitan laurate (Park et al., 2010), bovine serum albumin (Li et al., 2014), pluronic F127 (Cheng and Han, 2013) was used to modify the graphene derivatives by non-covalent interactions. However, non-covalent immobilization can lead to the leaking or fouling of proteins or bioreceptors from the surface of graphene derivatives.

The chemical functionalization of GO is based on using cross-linkers and was selected based on the functional units of the nanomaterials. Glutaraldehyde, a common cross-linker was used to immobilize enzymes on reduced graphene oxide decorated with cerium dioxide (Mukherjee et al., 2023). The carboxyl groups on GO were targeted mainly by using 1-ethyl-3-(3-dimethyl aminopropyl) carbodiimide (EDC) to form highly reactive O-acylisourea (Gao and Kyratzis, 2008). Hydrolysis and substitution reaction form a strong amide bond with N-hydroxysuccinimide (NHS) to form an open amine group on the surface suitable for protein immobilization. This method has demonstrated successful immobilization of BSA and enzymes, such as trypsin and glucose oxidase etc. Improper immobilization of enzymes and cross-linkers is detrimental as they can reduce the catalytic activity. Blocking the active sites of the enzyme or antibody with the cross-linker can directly hinder operational capability.

Hybrid graphene derivatives, rGO were doped with nanoparticles to prevent restacking of the nanosheets, providing high surface area by enhancing electron transfer and electron mobility. The metal nanoparticles were incorporated into graphene derivatives using reducing agents such as hydrazine hydrates and $NaBH_4$. The unique advantage of depositing nanomaterials is their ability to bind biomolecules, thereby improving stability. Herein, the nanomaterials act as immobilization carriers adding different properties, such as magnetism, and conductivity, and preparing the graphene nanocomposites for extensive applications as nanobiocatalytic bases (Verma et al., 2013). Therefore, these 2D graphene derivatives ideally constitute a nanosystem in biosensing and offers the potential to revolutionize futuristic diagnostics for cancer treatment.

4. Graphene-based biosensors for different types of cancer biomarkers

4.1. Oral cancer

Oral cancer (OC) is an aggressive form of cancer spreading among the tonsils, tongue, pharynx, lips, and mouth resulting from a combination of factors such as lack of awareness, high abundance of tobacco products, lack of early detection, and insufficient prognosis (Shrivastava et al., 2014). The detection of OC depends on invasive techniques such as an incisional biopsy to assess the histological condition of the concerned tissue (Cervino et al., 2019). Studies have proven the benefit of devising non-invasive electrochemical biosensors to reliably and sensitively detect oral cancer biomarkers in very low concentrations with high specificity in salivary samples (Labib et al., 2016; Kang et al., 2010).

CYFRA21-1 is a clinically significant biomarker for oral squamous cell carcinoma (OSCC), one of the most common forms of malignant tumors in the mouth (Pujol et al., 1993; Yamamoto et al., 1997). An elevated expression level of CYFRA21-1 (17.0 ± 2.0 ng mL^{-1}) in saliva samples compared to a healthy individual (3.80 ng mL^{-1}) is implicated in an insurgence of oral malignancy (Tiwari et al., 2017). Interestingly, CYFRA21-1 is also implicated in high levels during the progression of lung and bladder cancers (Pujol et al., 1993; Yamamoto et al., 1997; Tiwari et al., 2017; Sanchez-Carbayo et al., 1999). Several studies have demonstrated strategies to fabricate electrochemical biosensors for the detection of the CYFRA21-1 antigen. Kumar and co-workers

conceptualized an electrochemical biosensor for the selective detection of CYFRA21-1 using differential pulse voltammetry (DPV) and verified the detection in samples collected from OC patients (Kumar et al., 2016). Zirconium oxide (ZrO_2) has been previously used as a transducer due to its oxygen moiety, favorable charge transfer, and promising biocompatibility (Das et al., 2011; Liu and Lin, 2005). The prepared device, employed on an indium tin oxide (ITO) platform where rGO was functionalized with zirconia nanocrystals and (3-aminopropyl)triethoxysilane (APTES), improved the heterogeneous electron transfer, thereby indicating faster electron transfer kinetics than only ZrO_2 (Fig. 2(a)). By using an anti-CYFRA21-1 antibody for selective detection, the prepared biosensor demonstrated a very low limit of detection (LOD) of 0.122 ng mL^{-1} and a wide linear range (2.0–22.0 ng mL^{-1}). The selectivity of detection was tested in the presence of nonspecific biomarkers or chemical molecules, such as carcinoembryonic antigen (CEA), glucose, NaCl, etc., that had negligible effects on interference during detection. Moreover, the prepared sensor demonstrated 94 % of its initial peak value when tested 8 weeks after preparation, demonstrating its stability. Very recently, the same team of researchers prepared a similar immunosensor with slight modifications to stabilize zirconia nanocrystals (Kumar et al., 2019). In this effort, before functionalization on rGO sheets, zirconia NPs were doped with yttrium, which stabilized the crystal structure of the former, enhancing the stability and ionic conductivity of the sensing platform. The fabricated biosensor demonstrated efficient and highly selective detection of CYFRA21-1 in a wider linear range (100 fg mL^{-1} to 50.0 ng mL^{-1}) and a LOD of 7.20 pg mL^{-1}. The specificity of the biosensor was tested in the presence of known interferents and other salivary molecules, where it yielded negligible interference (0–1 %), successfully demonstrating high selectivity. In a similar effort to detect CYFRA21-1, a label-free electrochemical immunosensor was developed using nanocubes of cerium oxide ($ncCeO_2$) doped in rGO (Pachauri et al., 2018). CeO_2 has gained scientific interest due to its high isoelectric point (IEP 9.0), superior catalytic ability (Cheng et al., 2011), large surface area, and good biocompatibility (Strobel et al., 2014). In this study, an rGO matrix was used to stabilize $ncCeO_2$ on the surface and further functionalized with anti-CYFRA21-1 antibody. The electrochemical measurements showed a broad linear detection range of 0.625 pg mL^{-1} to 15.0 ng mL^{-1}. The fabricated immunosensor was proven to be effective in detecting the biomarker in antigen-spiked saliva samples and demonstrated high specificity in the presence of interferents such as glucose, NaCl, and other biomarkers. However, antigen-spiked samples do not always correspond to the true characteristics of a real sample, and application against patient saliva samples was not reported in this study. CYFRA21-1 was also detected by using a conductive multilayer formed by AuNPs and amino-substituted-pyrrole polymer (PyAmm) electropolymerized on the ITO platform where AuNPs were cross-linked by glutaraldehyde (Aydin et al., 2023). The deposited AuNPs provided enhanced conductivity and superior electron transfer.

Interleukins (ILs) are naturally occurring cellular messenger proteins called cytokines and are important for regulating cell growth, differentiation, and the immune response (Akdis, 2011). Deregulated expression levels of several IL molecules have been correlated with tumorigenesis and malignancy. In cancerous cells, overexpressed IL-8 stimulates the production of serine and cysteine proteases, which reduces cell attachment and results in an increase in circulating tumor cells (CTCs) (Akdis, 2011). The level of IL-8 in OSCC patients (720 pg mL^{-1}) is significantly higher than the basal level (250 pg mL^{-1}) in healthy individuals (St John

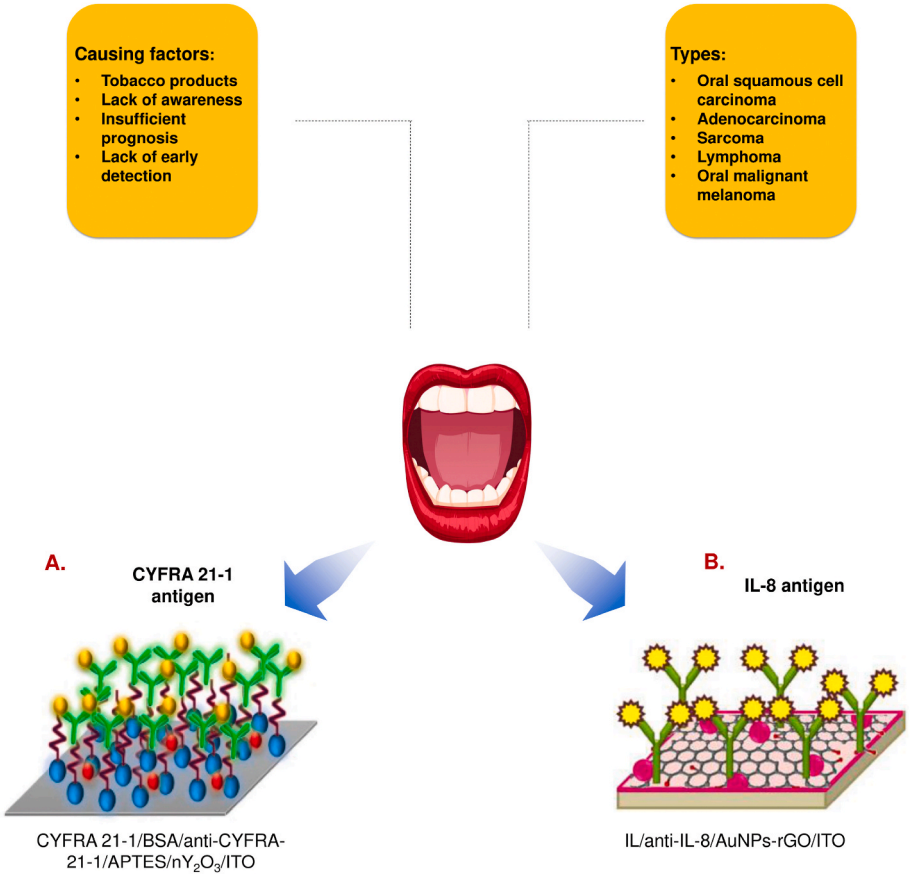

Fig. 2. Different types and factors causing oral cancer (OC). **(a)** Illustration of the fabricated immunosensors to detect CYFRA21-1 (reproduced with permission from Ref. (Kumar et al., 2019), Creative Commons Attribution (CC BY) license) and **(b)** IL-8 antigen (reprinted (adapted) with permission from Ref. (Verma et al., 2017), copyright 2017 American Chemical Society).

et al., 2004). Verma and colleagues developed an immunosensor using Au NPs on an rGO matrix for the rapid detection of IL-8 in spiked saliva samples (Fig. 2(b)) (Verma et al., 2017). Due to possessing a large surface area and high electrical conductivity, Au NPs are beneficial for electrochemical analyses. The prepared sensor promisingly demonstrated highly specific detection of IL-8 with a very low LOD (72.7 ± 0.2 pg mL^{-1}). The selectivity of detection was investigated by exposure to different cancer biomarkers, such as h-TERT and CD59. The results obtained by DPV measurement showed a negligible change in the output signal, indicating no interaction between the sensor surface and interferents. Most recently, the same research group reported a modified model of the earlier reported sensor where Au NPs were replaced by zinc oxide-rGO (Verma and Singh, 2019). This effort proved to be beneficial, as the reported biosensor exhibited a lower LOD (51.0 ± 1.0 pg mL^{-1}) with a wider linear range. The synergistic effect of rGO and Au NPs exhibited a fast response due to improved electron transfer behavior, thereby increasing the sensitivity of the sensing platform. A summary of developed electrochemical biosensors and their performances is presented in Table 3.

4.2. Lung cancer

Lung cancer (LC) is a rapidly metastasizing malignant tumor growing in respiratory bronchioles, bronchi, and alveoli. Clinically significant biomarkers of LC include cellular signaling proteins and genetic mutations that lead to carcinogenesis irrespective of the individual's preference for smoking. Tremendous efforts have been made by various research groups to use the advantages of electrochemical biosensing principles to detect lung cancer biomarkers at various stages for better prognosis and disease management. In the following section, strategies for the fabrication of antibody-based and DNA-based nano-biosensors to detect different clinically significant biomarkers are discussed.

Recently, the fabrication of an aptamer-based biosensor was reported to detect epidermal growth factor receptor (EGFR) protein using the principles of paper-based microfluidics and electrochemical measurements (Fig. 3(a)) (Wang et al., 2020). This reported study utilized a screen-printed electrode (SPE), and the surface was further modified with aminated GO, thionine, and Au NPs. The modified nanocomposite enhanced the generation of electrochemical signals and provided a conducive environment for anti-EGFR aptamer immobilization, which was covalently immobilized on the modified electrode by Au-S bonding. A low signal was reported from the prepared aptamer-antigen immunocomplex as it was insulative, restricting electron transfer from the sample to the working electrode revealed by the electrochemical characterization. When tested with antigen-spiked serum samples, the aptasensor demonstrated effective and sensitive detection of EGFR with a LOD of less than 4.99 pg mL^{-1}. The device showed excellent specificity to detect EGFR in the presence of potential interferents.

Neuron-specific enolase (NSE) is found at high expression levels in the serum of SCLC-affected patients (Yang et al., 2019); hence, it is an appropriate target for the diagnosis of the disease. Several studies have reported fabrication strategies to prepare antibody-based and low-cost nanosensors for the rapid detection of NSE. For example, in a recent study, researchers utilized reduced-molybdenum disulfide (r-MoS_2) in combination with rGO to create an ITO electrode coating 2D surface (Khatri and Puri, 2022). In this nanosensor, rGO provided functional groups to bind biomolecules, while r-MoS_2 was utilized as a supporting matrix to hold the biomolecules in place and to facilitate the rapid transfer of electrons. The large electroactive surface area in the sensing platform ensured a wide detection range of 100 pg mL^{-1} to 100 ng mL^{-1}, and the lowest detected value by the EIS technique was 1.00 ng mL^{-1}. The biosensor successfully exhibited high reproducibility and specificity

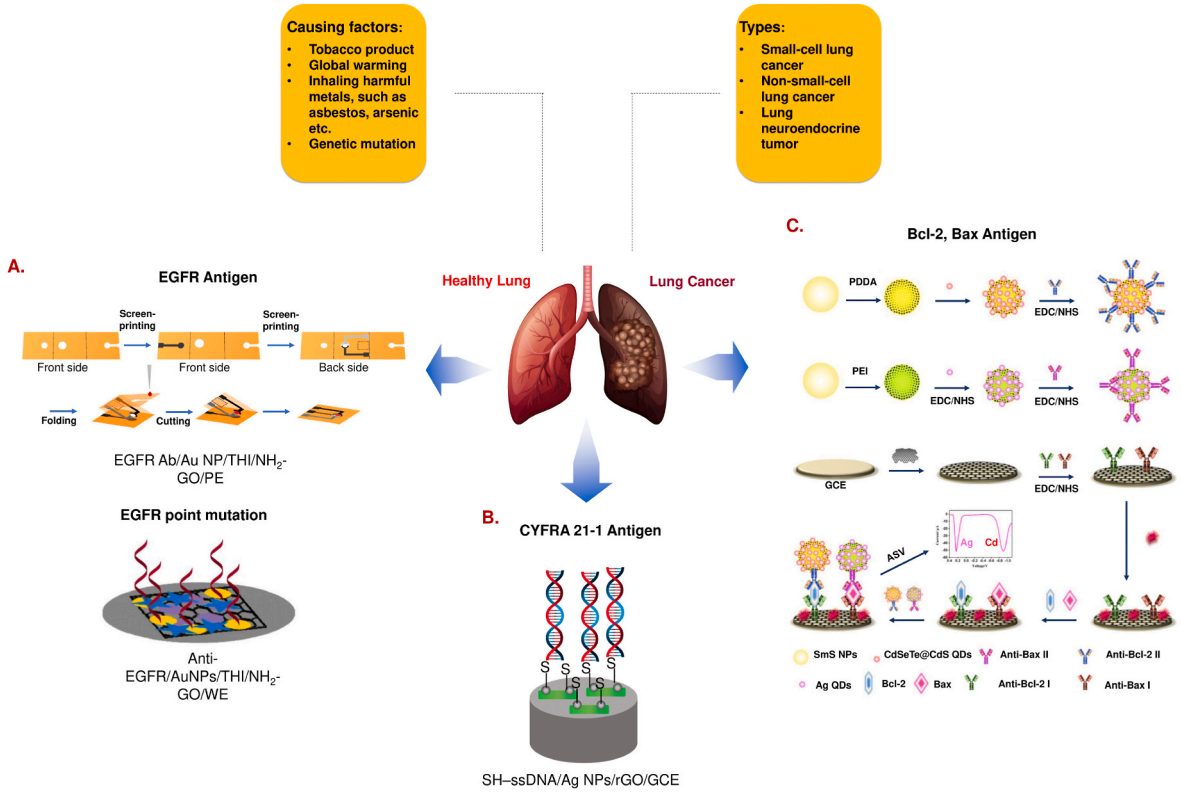

Fig. 3. Different types and causative factors of LC. **(a)** Schematic illustration of paper electrode development to detect EGFR-Ab (reproduced with permission from Ref. (Wang et al., 2020), copyright 2020 Creative Commons Attribution (CC BY) license), **(b)** DNA-based nanosensor for the detection of CYFRA21-1 antigen (reproduced with permission from Ref. (Jafari-Kashi et al., 2022), copyright 2022 Elsevier), and **(c)** schematic illustration for the fabrication of a dual-detection immunosensor for the detection of Bcl-2 and Bax protein (reprinted (adapted) with permission from Ref. (Zhou et al., 2016), copyright 2016 American Chemical Society).

in the presence of interferents, such as cardiac troponin I, myoglobin, and NaCl; however, its application against real samples was not reported. In another effort, Fang and co-workers used a three-dimensional porous graphene material (3D-GN) coupled with starch as a stabilizer to fabricate an immunosensor platform (Fang et al., 2019). The porous nature of 3D-GN provided a large surface area, made it easier for the NPs and biomolecules to diffuse, and facilitated efficient retention. The functional groups of chitosan coating provided MoS_2 to act as anchors for antibody immobilization, and Ag NPs were deposited to enhance the efficiency of detection due to their unique abilities, such as lower oxidation potential, increased biocompatibility and the ability to decrease potential interference, thereby increasing sensitivity. Herein, the glutaraldehyde acted as a cross-linker for the immobilization of the primary antibody. The as-prepared immunosensor showed an extremely low detection limit of 8.00 fg mL^{-1} and a linear range of detection of 20.0 pg mL^{-1} – 35.0 ng mL^{-1} for NSE. The developed sensor was found to be reliable, as the detection was verified in a comparative analysis between healthy and LC-affected patient serum samples.

DNA-based biosensors are extremely versatile yet accurate tools for the detection of single or multiple DNA biomarkers. Strategies for electrochemical detection of genomic DNA fragments or circulating tumor DNA clinically significant to LC have been reported. A DNA-based nanosensor was developed for the detection of CYFRA21-1 DNA and demonstrated low LOD and high specificity (Jafari-Kashi et al., 2022). The DNA capture probes were bound and stabilized on the rGO that was used as a matrix (Fig. 3(b)). To enhance the sensitivity of the device, it was further modified with polypyrrole (PPy) and Ag NPs by electropolymerization. PPy is a conductive polymer that offers useful features such as good biocompatibility and excellent electrical conductivity (Aydın et al., 2020). The capture probe was attached to the matrix by covalent Ag-S bonding providing excellent stability, but the authors have provided doubts regarding the elimination of adsorbed molecules. The sensor demonstrated the ability to efficiently identify and hybridize CYFRA21-1 target DNA with a LOD of 2.40 fmol L^{-1} in a linear range of 10.0 fmol L^{-1} to 1.00 μmol L^{-1}. An RSD% value of less than 5.4 % based on independently prepared electrodes confirmed the high reproducibility of the developed method. In another report, a paper electrode was prepared and modified with rGO or MoS_2 nanosheets along with Au NPs for the detection of microRNA-155 and microRNA-21 (Torul et al., 2021). Both of these miRNAs are clinically correlated with the prognosis of LC. This nanosheet-based device showed effective detection and hybridization of miRNAs with the capture probes on the electrode surface. Voltammetric measurements presented LODs for miRNA-21 of 12.0 and 51.7 nmol L^{-1} when rGO-Au NPs were used in the platform, while in the case of miRNA-155 in the Au NP/MoS_2-modified paper electrode, the values were 25.7 and 59.7 nmol L^{-1}. The selectivity of the sensing platform was tested in the presence of nonspecific microRNA samples.

In a notable effort, a sandwich-type electrochemical immunosensor was developed for the efficient simultaneous detection and quantification of Bcl-2 and Bcl-2-associated X protein (Bax) in a single sensing device (Zhou et al., 2016). In clinical practice, the cellular levels of Bcl-2 and Bax are often checked to analyze the effects of cancer drugs on tumor cells. The surface of rGO was modified with primary antibodies against Bcl-2 and Bax on the electrode surface, while Ag-based or Cd-based core@shell quantum dots (QDs) were prepared to carry a secondary antibody specific to bound antigens and served as signal probes (Fig. 3(c)). The mesoporous silicon dioxide nanoparticle has a rough surface area and can be charged using PEI and PDDA to enhance its surface area and absorption capability. Ag^{+} and Cd^{2+} ions were released upon binding of the secondary antibody complex to the antigen. The release was measured using anodic stripping voltammetry (ASV). An unfavorable working environment can be a drawback, as important fabrication steps for this developed biosensor were based on the adsorption of capture probes that are likely to desorb. Notably, the cellular levels of Bcl-2 and Bax were indirectly measured and then correlated with the oxidation peak current of released ions. The linear detection range for proteins was obtained as 1.00–250 ng mL^{-1}. According to the signal-to-noise ASV response of the standard samples, the detection limit of the immunosensor was measured to be approximately 1.00 ng mL^{-1}. Table 4 shows a summary of developed electrochemical biosensors for lung cancer detection and lists their detection abilities.

4.3. Colorectal cancer

Colorectal cancer (CC) refers to tumors originating from the colon or rectum area. In conventional medical practices, diagnosis is performed with various techniques, such as colonoscopy, capsule endoscopy, and CT colonoscopy. To further simplify the detection process and minimize invasive procedures, several attempts have been made to strategize electrochemical biosensors targeting CC biomarkers.

Epithelial cell adhesion molecules (EpCAMs) are glycosylated transmembrane proteins expressed on the surface of circulating tumor cells (Keller et al., 2019). Many studies have correlated the overexpression of EpCAMs in different carcinomas, such as colon, rectum, prostate, stomach, and breast carcinomas: these molecules are now considered prognostic biomarkers for the diagnosis of colorectal cancer (Porcel et al., 2019; Yoon et al., 2014). Conventional techniques such as cytometry and ELISA are used to quantify the level of EpCAM. Using nanomaterials, several reports have described the preparation of a sensitive biosensor for the detection of EpCAM (Arya et al., 2013; Ortega et al., 2015). Very recently, a biosensing platform has been reported using rGO modified with TiO_2 NPs (Jalil et al., 2020). The deposition of rGO-TiO2 nanocomposites on the ITO electrode was carried out electrophoretically, and the anti-EpCAM antibody was covalently immobilized on the surface for the detection of the antigen (Fig. 4(a)). The immunosensor exhibited a wide detection range of 10.0 pg mL^{-1} to 60.0 ng mL^{-1}, and the LOD was 6.50 pg mL^{-1}. When tested against antigen-spiked serum, the immunosensor showed sufficiently high sensitivity and recovery rates.

CEA is a reliable biomarker for CC and is found at a very minimal level in the blood of healthy individuals. The rise in serum CEA levels has been linked with many major cancers, such as colon and lung cancers (Perkins et al., 2003). Studies have reported the preparation of various antibody- or aptamer-based noninvasive biosensors for the reliable detection of CEA (Xiang et al., 2020; Paimard et al., 2020; Li et al., 2020; Jin et al., 2014). A portable sensor was reportedly developed by point-to-point fabrication using a 2D rGO layer as the transport base for the detection of CEA at room temperature (Joshi et al., 2022). The conductive rGO base layer was fabricated with poly [(1, 4-phenylene)-alt-(3,6-(1,2,4,5-tetrazine)3,6-(1,2,4, 5-dihydrotetrazine))] (PhPTz), an immobilizing matrix for the incorporation of anti-CEA antibodies (Fig. 4(b)). The nitrogen-rich property of PhPTz provided several advantages to the fabricated system, such as efficient immobilization of anti-CEA antibody through H-bonding between the peptide and N-glycan units, and the variation in charge density was transported to the rGO base layer following Ag-Ab interaction. The developed sensors were tested with various concentrations (from 250 fg mL^{-1} to 800 ng mL^{-1}) of CEA antigen in spiked fetal bovine serum samples, and the change in current was recorded upon CEA binding at room temperature. The responses of the sensors were found to be highly reproducible even when tested on devices with varied baseline currents.

Recently, Shang et al. reported the fabrication of a low-potential driven transducer composed of graphene-ionic liquid decorated with PtPd NPs (GN-IL-PtPd) (Shang et al., 2021). This hybrid nanocomposite efficiently immobilized Ab1 and hydrothermally prepared MoS_2 nanoflowers were used to form Ab2 nano-complexes. The electrochemiluminescent (ECL) behavior of $[Ru(bpy)_3]^{2+}$ was observed following the formation of a sandwich-type interaction in the presence of CEA (Fig. 4(c)). The $[Ru(bpy)_3]^{2+}$ was able to enhance and stabilize the ECL output at a low potential magnitude of 0.05 V, which enhances the selectivity. The synergistic effect of the Pt and Pd bimetallic

Table 4
Published works about electrochemical detection of lung cancer biomarkers.

Analyte	EC techniques	Fabrication	LOD	Sensitivity	Range of detection	Ref.
NSE	CV, EIS	BSA/anti-NSE/r-MoS_2-rGO/ITO	1.0 fg mL^{-1}	2.32 μA ng^{-1} mL cm^{-2}	100 pg mL^{-1} – 100 ng mL^{-1}	Khatri & Puri (2022)
NSE	CV, DPV, EIS	MIP-Poly (DPIMBr)/GNA-MVIMBF4/GCE	2.60 pg mL^{-1}	65.2 μA ng^{-1} mL cm^{-2}	10.0 pg mL^{-1} – 1.00 ng mL^{-1}	Wang et al. (2018)
NSE	LSV, EIS,	Ab2–OMCSi–Au/CS/3D-GNS/GCE	8.0 fg mL^{-1}	–	20.0 fg mL^{-1} – 35.0 ng mL^{-1}	Fang et al. (2019)
Bcl-2, Bax	ASV	NCs(QDs)-SmS/Ab2/Antigen/Ab1/rGO/GCE	1.00 ng mL^{-1}	NR	1.00–250 ng mL^{-1}	Zhou et al. (2016)
CYFRA21-1 DNA	CV, EIS, DPV	ssDNA/Ag NPs/rGO/PPy/GCE	2.14 fmol L^{-1}	–	10.0 fmol L^{-1} – 1.00 μmol L^{-1}	Jafari-Kashi et al. (2022)
EGFR	CV, DPV	EGFR Ab/Au NP/THI/NH_2-GO/PE	5.0 pg mL^{-1}	NR	50.0 pg mL^{-1} – 200.0 ng mL^{-1}	Wang et al. (2020)

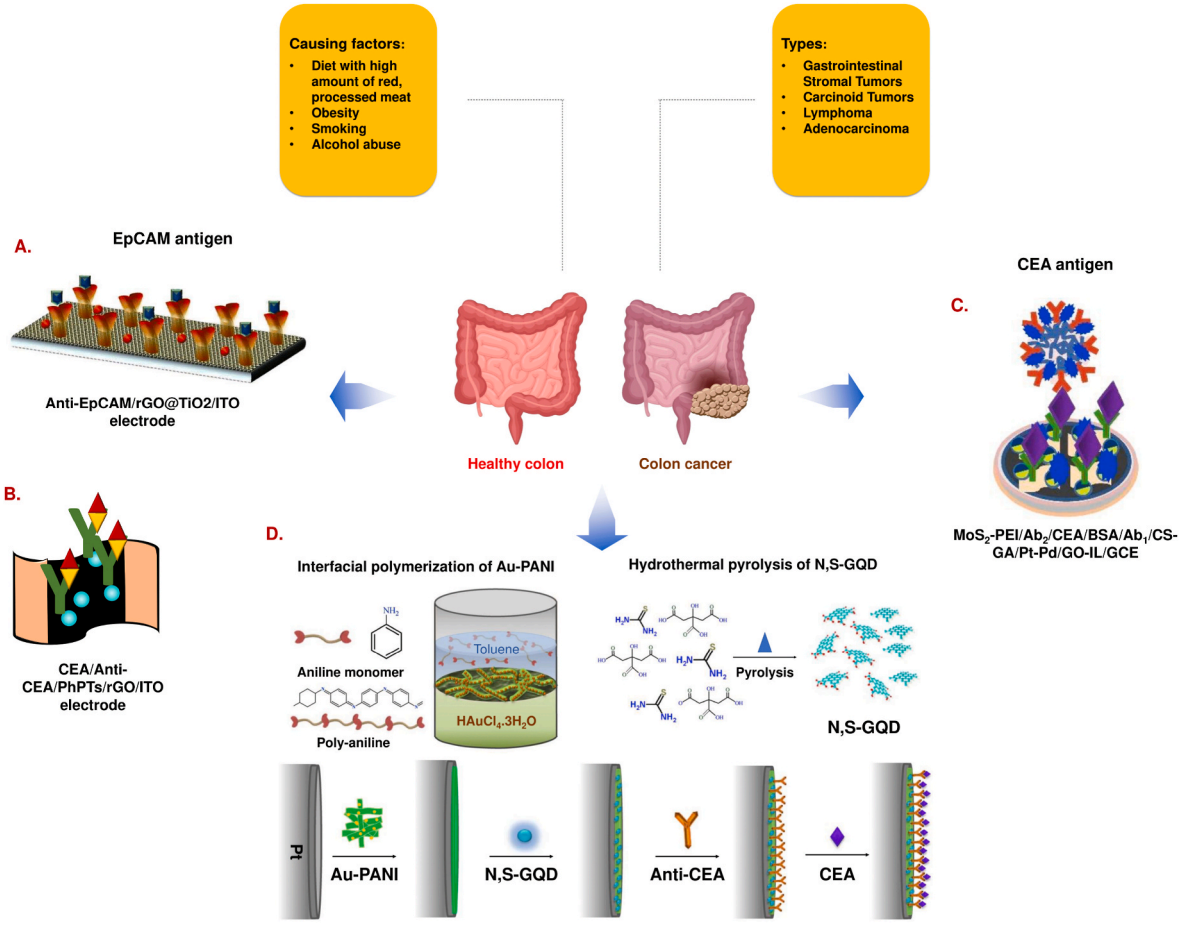

Fig. 4. Schematic presentation of colorectal cancer. **(a)** Fabricated sensor for EpCAM detection (reproduced with permission from Ref. (Jalil et al., 2020), copyright 2020 Springer Nature), **(b)** fabricated immunosensor for the detection of CEA (reproduced with permission from Ref. (Joshi et al., 2022), copyright 2020 Creative Commons Attribution 4.0. License), **(c)** immunosensor with electrochemiluminescence behavior (reproduced with permission from Ref. (Shang et al., 2021), copyright 2021 Springer Nature), and **(d)** schematic illustration of CEA detection by using electrochemical deposition of Au-PANI (reproduced with permission from Ref. (Ganganboina and Doong, 2019), copyright 2019 Creative Commons Attribution 4.0. License).

composite in GN-IL-PtPd for the measured ECL signal was significantly higher than those of the individual NPs (GN-IL-Pt or GN-IL-Pd) at −0.15 V (vs. Ag/AgCl). The effective detection of CEA was demonstrated based on the sandwich-type interaction and the quenching effect of the MoS_2 nanoflowers. The linear detection range for CEA was reported to be from 1.00 fg mL^{-1} to 1.00 ng mL^{-1} with a detection limit of 0.540 fg mL^{-1}, and the observed detection was verified in antigen-spiked human serum samples.

Using carbon quantum dots (carbon QDs) and a nanocomposite of gold-polyaniline (Au-PANI), a highly sensitive impedimetric biosensor was developed for the detection of CEA (Haglund et al., 1994). PANI is an interesting organic conductive polymer with a large surface area that is especially advantageous for loading with different molecules. In that study, the platinum electrode was coated with Au-PANI, and further GQDs with thiol groups on the surface were immobilized by considering the interaction chemistry of Au-thiol (Fig. 4(d)). Indeed, GQDs were of particular importance in this biosensor for amplifying the signal and for the attachment of the anti-CEA antibody. The principal mechanism for the detection of CEA is the change or blockage in the electron transfer of co-doped GQD-Au-PANI after the addition of antigen CEA by forming

the antigen-antibody bio-conjugation. In terms of the electrochemical measurements, this immunosensor exhibited superior sensitivity and an extended detection range compared to other developed or published biosensors for CEA. In the assays conducted by the researchers, a linear detection range of 500 pg mL^{-1} – 1.00 pg mL^{-1} and LOD of 10.0 pg mL^{-1} were observed. The developed immunosensor exhibited similar efficiency when tested for detection in human serum samples spiked with increasing concentrations of CEA antigens.

Very recently, a label-free nanostructured-based immunosensor was reported and the antifouling properties were emphasized. The GO decorated with electrodeposited Au nanoflower nanostructure (GO@Au-NS) was fabricated on fluorine-doped tin oxide to detect miR-223 CC biomarker (Akbari et al., 2023). Antifouling properties were enhanced by hydrophobicity or hydrophilicity on the electrode surface, resulting in a higher hydrophilicity index by the formation of a hydration layer on the surface. The GO nanosheets were activated with EDC/NHS to increase their solubility for better attachment of the functionalized GO. The electrodeposition of Au-NF on the GO shows an excellent hydrophilicity index with strong antifouling properties. The Au nanoflowers deposition was advantageous as the thiolate ss-DNA capture probe was covalently bonded. The hybridized cap-223 capture probe was able to detect miRNA-223 with a LOD of 0.012 aM. Moreover, it was also reported that this fabricated biosensor was able to distinguish a mismatch sequence of miRNA-223 in human serum samples, manifesting excellent selectivity and sensitivity properties. A summary of developed electrochemical biosensors for colorectal cancer detection is presented in Table 5.

4.4. Pancreatic cancer

In conventional practice, physicians use various imaging and biopsy techniques to diagnose pancreatic cancer (PC) in an advanced stage when a complete cure is rarely possible. Carbohydrate antigen 24-2 (CA 24-2) is a highly specific tumor biomarker of pancreatic and colorectal cancers (Haglund et al., 1994). A label-free novel immunosensor to detect CA 24-2 was prepared using nanocomposites of rGO, Au, and palladium (Pd) (Du et al., 2019). The bimetallic nanocomposite Au-Pd in this immunosensor provided a large smooth surface area and was able to facilitate efficient electron transfer. A sensing platform was prepared to consist of rGO modified with Au-Pd and anti-CA 24-2 antibody (Fig. 5 (a)). The prepared immunosensor successfully detected the target analyte in spiked human serum samples with high sensitivity. Electrochemical measurements showed a linear detection range of 1.0×10^{-3} – 1.0×10^{4} U mL^{-1}, and the LOD was approximately 1.0×10^{-3} U mL^{-1}. The reported biosensor exhibited high reproducibility and excellent specificity in the presence of nonspecific electroactive components, such as dopamine and ascorbic acid.

Matrix metalloproteinase-7 (MMP-7) is an important enzyme responsible for the degradation of proteins in the extracellular matrix. Significantly high levels of MMP-7 expression in serum samples have been clinically referred to as one of the prognostic factors of PC (Szarvas et al., 2010). A biosensor was developed with GO and two-dimensional MoS_2 on an SPCE for label-free detection of MMP-7 (Yaiwong et al., 2021) (Fig. 5(b)). The nanocomposite deposited onto the SPCE increased the effective large surface area and enhanced the electron transfer rate. Moreover, methylene blue (MB) was used to amplify the output signal of the immunosensor. The developed NC was modified with MB by adsorption, and the anti-MMP-7 antibodies were immobilized via electrostatic interactions. A decrease in the output current was observed for the MB response for MMP-7 binding onto the immunosensor complex. The developed sensor exhibited a linear logarithmic range of 10.0 pg mL^{-1} – 75.0 ng mL^{-1} with a limit of detection (LOD) of 7.00 pg mL^{-1} for MMP-7. Moreover, the reliability of the prepared immunosensor was investigated against spiked human serum samples but the weak bonding, such as electrostatic interaction and adsorption during fabrication, can diminish or lead to reduced working ability at unfavorable conditions.

A tyrosine kinase, pseudopodium enriched atypical kinase 1 (PEAK1), was found to be significantly overexpressed specifically in PC, where it plays an important role in proliferation and metastasis (Strnadel et al., 2017). A paper-based microfluidics platform was devised by Prasad and colleagues for the detection of the PC biomarker PEAK1 in trace amounts (Prasad et al., 2020) (Fig. 5(c)). A paper-based screen--printed electrode (SPE) surface was fabricated with GO, and as a detection method, anti-PEAK1 antibody was immobilized on the surface. Additionally, Au NPs were used on the sensing device to enhance the generated signal. The prepared device reliably detected the specific antigen with a LOD of 10.0 pg mL^{-1}, with successful reproduction in spiked human serum samples, and a wide linear range was observed (10.0 pg mL^{-1} – 1.00 μg mL^{-1}).

Carbohydrate antigen 19-9 (CA 19-9) is another tumor marker that was found to be highly overexpressed in PC (Du et al., 2003). In an effort to prepare a fast, low-cost, and reliable detection tool for CA 19-9, SPEs were fabricated with multi-layered carbon structures and GO, demonstrating reproducible detection based on antibody-antigen interactions (Ibáñez-Redín et al., 2019) (Fig. 5(d)). The deposition of carbon nanomaterials greatly enhanced the analytical properties of the sensor and provided a large surface area to bind antibodies in high amounts. The immunosensor showed satisfactory analytical performance with a LOD of 1.20×10^{-1} U mL^{-1} and a linear range of detection from 3.00×10^{-1} to 100 U mL^{-1} with respect to whole cell lysates of colorectal adenocarcinoma. No significant change in the output signal was reported in the presence of possible interferents, demonstrating the sensor's ability for specific detection. It is worth noting that due to the fabrication of this immunosensor on a flexible screen-printed material, it can be used as a non-invasive biosensor, allowing it to be placed on the skin to analyze analytes present in sweat or saliva as samples. A summary of prepared electrochemical biosensors for pancreatic cancer utilizing different biomarkers is presented in Table 6.

4.5. Breast cancer

Breast cancer (BC) is one of the most common causes of cancer fatalities worldwide. Various endogenous and lifestyle factors are also

Table 5
Published works about graphene-based biosensors detecting colorectal cancer biomarkers.

Analyte	EC techniques	Fabrication	LOD	Sensitivity	Range of detection	Ref.
CEA	CA	CEA/anti-CEA/PhPTz-rGO/ITO	8.75×10^{-7} pg mL^{-1}	NR	250 fg mL^{-1} – 800 ng mL^{-1}	Joshi et al. (2022)
CEA	CV, EIS, ECL-time curve	MoS_2 NFs-Ab_2//CEA//Ab_1/GA/CHI/GN-IL-PtPd/GCE	0.540 fg mL^{-1}	NR	1.00 fg mL^{-1} – 1.00 ng mL^{-1}	Shang et al. (2021)
CEA	CV, EIS	Pt-PANI-Au/N,S-GQDs/anti-CEA	10.0 pg mL^{-1}	NR	500 pg mL^{-1} – 1000 ng mL^{-1}	Ganganboina & Doong (2019)
EpCAM	CV	anti-EpCAM/LC-SPDP/Au electrode	1.00×10^{5} cells mL^{-1}	NR	1.00×10^{5}–1.00×10^{8} cells mL^{-1}	Arya et al. (2013)
EpCAM	EIS, DPV	anti-EpCAM/rGO@TiO_2/ITO	6.50 pg mL^{-1}	3.24 μA mL ng^{-1} cm^{-2}	10.0 pg mL^{-1} – 60.0 ng mL^{-1}	Jalil et al. (2020)

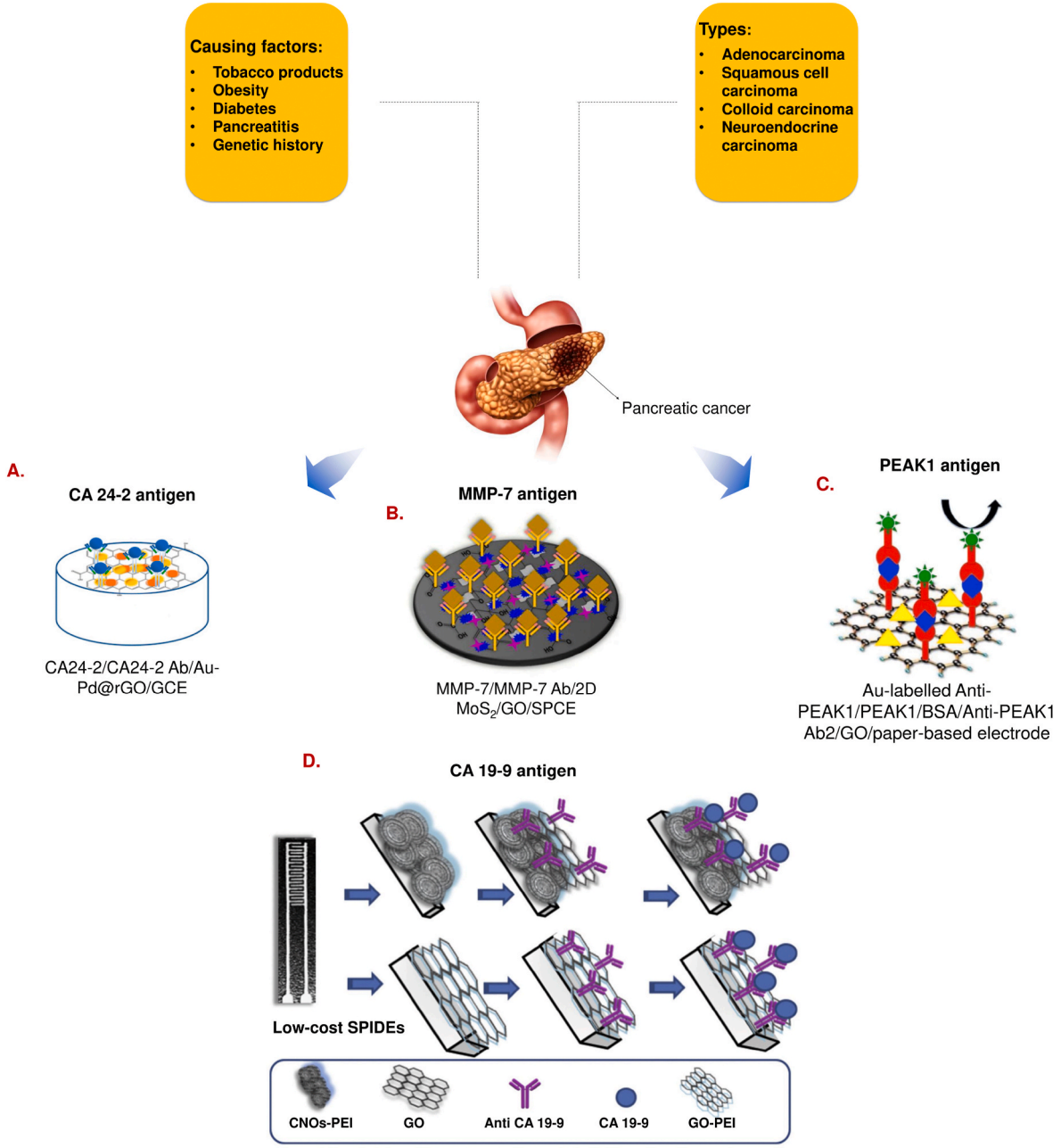

Fig. 5. Fabrication of different sensors for the detection of biomarkers for pancreatic cancer. **(a)** Immunosensor for the detection of CA24-2 (reproduced with permission from Ref. (Du et al., 2019), copyright 2019 Creative Commons Attribution (CC BY) license), **(b)** fabricated sensor for the detection of MMP-7 (reproduced with permission from Ref. (Yaiwong et al., 2021), copyright 2021 Elsevier), **(c)** sandwich-based immunosensor for the detection of PEAK1 antigen (reproduced with permission from Ref. (Prasad et al., 2020), copyright 2021 Elsevier), and **(d)** immunosensor for the detection of CA19-9 (reproduced with permission from Ref. (Ibáñez-Redín et al., 2019), copyright 2019 Elsevier).

Table 6
Published works about electrochemical detection of pancreatic cancer biomarkers.

Analyte	EC techniques	Fabrication	LOD	Sensitivity	Range of detection	Ref.
CA 24-4	CV, DPV	rGO-Au-Pd-anti-CA_{24-2}-BSA/GCE	1.0×10^{-3} U mL^{-1}	4.24 μA	1.00×10^{-3} – 1.00×10^{4} U mL^{-1}	Du et al. (2019)
CA 19-9	CV, DPV	HRP-CA_{19-9}/anti-CA_{19-9}/Ti-sol-gel/GE	2.68 U mL^{-1}	1.92 μA mL U^{-1} cm^{-2}	3.00–20.0 U mL^{-1}	Jin et al. (2014)
MMP-7	CV, EIS, DPV	BSA/anti-MMP-7/2D MoS_2/GO-modified SPCE	1.00×10^{-3} ng mL^{-1}	−28.2log ng mL^{-1} cm^{-2}	10.0 pg mL^{-1} – 75.0 ng mL^{-1}	Yaiwong et al. (2021)
PEAK1	CV, DPV	BSA/Anti PEAK1-GO-PPE	10.0 pg mL^{-1}	20.7log pg mL^{-1} cm^{-2}	10.0–1.00×10^{6} pg mL^{-1}	Prasad et al. (2020)

linked as probable causes of BC, such as inherited gene mutations in BRCA1 and BRCA2 (King et al., 2003), increasing age (Siegel et al., 2013), delayed menopause (Kelsey et al., 1993), obesity (Lahmann et al., 2004), long-term radiation exposure (Henderson et al., 2010), and alcohol consumption (Chen et al., 2011). Clinical diagnosis of BC includes mammography and other imaging techniques, such as MRI and ultrasound, and prognostic indications, such as the expression profiles of estrogen and progesterone receptors (Fitzgibbons et al., 2000) and epidermal growth factor receptor 2 (HER2) (Wolff et al., 2007; Goutsouliak et al., 2020).

Several efforts have been made by researchers to develop noninvasive and rapidly detecting biosensors for the early diagnosis of BC (Sharifi et al., 2020; Sadighbayan et al. 2019, 2019; Wang et al., 2020). Among the clinically prominent biomarkers of BC, HER2 is widely studied, and its overexpression has been reported in approximately 30 % of all BCs (Cho et al., 2003; Hartati et al., 2020). Overexpression of the HER2 extracellular domain can be detected through biopsy, immunohistochemistry, and fluorescence in situ hybridization. Non-invasive biosensors have also been proven to efficiently detect HER2 and rapidly correlate to disease conditions. A novel graphite electrode-based aptasensor (g-aptasensor) was constructed for the detection and determination of HER2 cancer cells (Sadeghi et al., 2022). A hybrid nanocomposite platform was fabricated on a graphite electrode by electrochemical synthesis of rGO nanosheets (rGONs). In situ oxidative cyclic voltammetry (CV) was performed from potential 0.0 to +0.3 V to form several layers of GO nanosheets (GON) on the graphite electrode. Later, CV from 0.0 to −1.6 V was applied to reduce the GON to form rGON, followed by electrochemical synthesis of rhodium NPs (RhNPs) by sweeping the potential between 0.0 and −0.8 V. The synergistic effect of the rGONs and RhNPs enhanced the electrochemical signal and sensitivity by increasing the conductivity and specific surface area. The stability of the formed G-quadruplex on the rGONs increased the strong covalent interaction between the aptameric strands and the HER2 tumor marker. It was reported that this fabricated g-aptamer had an excellent LOD value of 1.00 cell mL^{-1} concerning SKBR2 cells. The same research group reported the detection of the HER2 tumor marker by fabricating a nano-biosensor using a pencil graphite electrode modified by 2D functionalized GO (Sadeghi et al., 2022) (Fig. 6(a)). GO was also synthesized by electrochemical oxidation on the graphite surface and activated by using EDC/NHS for the immobilization of the anti-HER2 aptamer. The FGO increases the active sites due to fast electron transfer by increasing the active surface area of the electrode by increasing the reactivity of the modified electrode. The transducer layer along with the EDC/NHS strategy was suitable for the effective immobilization of aptamer strands through amide bonds, stabilizing to form a G-quadruplex and thereby increasing the selectivity and sensitivity for the detection of HER2. The fabricated sensor was capable of detecting the biomarker with a linear range of 500 pg mL^{-1} to 25.0 ng mL^{-1} and a LOD of 590 pg mL^{-1}. Interestingly, the prepared immunosensor was tested against patient serum samples and demonstrated reliable detection.

Cluster of differentiation-44 (CD-44) antigen is a transmembrane glycoprotein that exhibits multifunctional malignant behavior, including cell adhesion, proliferation, migration, differentiation, and signaling (Yan et al., 2015). A hybrid nanocomposite consisting of IL,

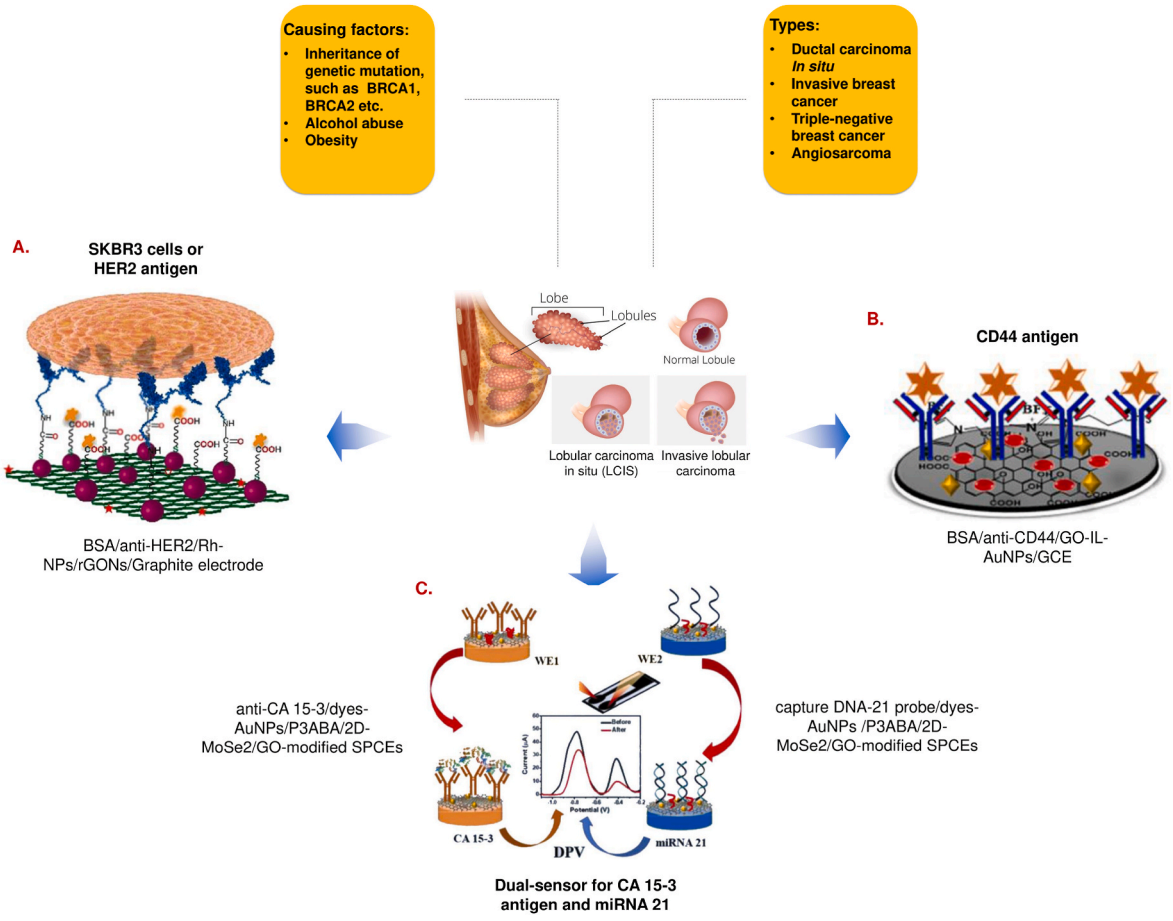

Fig. 6. Fabrication strategies of electrochemical biosensors to detect different BC biomarkers. (a) Immunosensor for the detection of HER2 antigen (reproduced with permission from Ref. (Sadeghi et al., 2022), copyright 2022 Creative Commons Attribution (CC BY) license), (b) biosensor for the detection of CD44 antigen (reprinted (adapted) with permission from Ref. (Ranjan et al., 2022), copyright 2022 American Chemical Society), and (c) schematic illustration for the fabrication of dual sensor for the detection of antigen CA 15-3 and miRNA 21 on an SPCE (reproduced with permission from Ref. (Pothipor et al., 2022), copyright 2022 Elsevier).

GO, and Au NPs was immobilized onto the GCE to form an immunosensing platform for the PoC detection of CD-44 antigen (Ranjan et al., 2022) (Fig. 6(b)). IL confers advantages, as it is biocompatible for CD44 immobilization and prevents leaching due to its adhesive nature. Moreover, IL prevents the agglomeration of NPs and thereby increases the stability of the sensing platform. The GO-IL and Au NPs collectively enhanced the electrical conductivity of the nanocomposites and increased the effective surface area favorable for the immobilization of anti-CD-44 Abs. The developed immunosensors reported a wide range of antigen detection (from 5.0 fg mL^{-1} to 50.0 μg mL^{-1}) with a LOD of 2.80 fg mL^{-1}, and the detection was reliably reproduced in human serum samples.

The role of microRNAs (miRNAs) in regulating various cellular signaling pathways and in the progression of disease conditions is well known. Deregulation of miRNA expression profiles has been linked with several cancer conditions (Babaei et al., 2020; Kashyap and Kaur, 2020). miRNA-21 is reported to be highly overexpressed in breast invasive carcinoma and hence plays an important role as a reliable biomarker for BC. miRNA-21 and cancer antigen 15-3 (CA 15-3) are two different kinds of breast cancer biomarkers that have been employed for the detection of cancer by using a dual-mode electrochemical biosensor (Pothipor et al., 2022). The dual-mode sensor acts as an immunosensor and DNA-based sensor. The biosensor was fabricated by using a poly (3-aminobenzylamine)/2D $MoSe_2$/GO nanocomposite-modified two--carbon SPE array (Fig. 6(c)). The electrodes were functionalized with redox probes individually added onto Au NPs by 2,3-diaminophenazine and toluidine blue. These redox probes along with Au NPs were employed to maintain and immobilize the anti-CA15-3 Ab and capture DNA-21 probes. The high electrical conductivity and the enhanced surface-to-volume ratio of the nanocomposite were found to be effective for the immobilization of antibodies and capture probes onto the modified electrode. The fabricated biosensor demonstrated good selectivity and higher sensitivity to target the two analytes, resulting in a label-free biosensor. The biosensor enabled detection limits of 1.40×10^{-1} U mL^{-1} and 1.20 fmol L^{-1} for CA 15-3 and miRNA-21, respectively, and successfully exhibited reliability of detection in spiked human serum samples. Table 7 summarizes developed electrochemical biosensors for the detection of breast cancer and presents their detection ranges.

4.6. Prostate cancer

Prostate cancer (PstC) is a malignancy involving prostate cells [114]. Although many genes have been implicated in the late state progression of PstC, notable mutations in BRCA1 and BRCA2 have been found along with BC (Tan et al., 2018). Engrailed-2 (EN2) protein is designated as a transcriptional repressor and serves as a reliable, well-studied biomarker for PstC (Pandha et al., 2012). EN2 exhibits strong binding affinity to the 5'-TAATTA-3' nucleotide sequence for the regulation of transcription. Exploiting this intrinsic property, an aptamer-based biosensor for the detection of EN2 was developed (Settu et al., 2017) (Fig. 7(a)). The aptamer containing the target TAATTA sequence was attached to the carbon-graphene electrode. The quantitative detection of the attached EN2 protein to the biosensor was performed by CV involving potassium ferricyanide (K_3 [$Fe(CN)_6$]). The interruptions in the redox reaction of K_3 [$Fe(CN)_6$] on the electrode surface due to the binding of free EN2 protein to the target sequence in the aptamer were converted into the quantitative measurement of EN2 concentration. In the electrochemical measurements under optimized conditions, the prepared biosensor successfully detected EN2 in a linear range of 35.0–185 nmol L^{-1} with a LOD of 33.8 nmol L^{-1}.

In conventional medicine, the diagnosis of PstC depends on checking prostate-specific antigen (PSA) levels in blood and biopsy of prostate tissue. Furthermore, PSA, also known as human kallikrein 3 (hK3), is one of the early serological biomarkers for PstC (Hernandez and Thompson, 2004). Recently, several efforts have been made to develop highly selective electrochemical biosensors for the detection of PSA with good sensitivity (Sharifi et al., 2019). To prepare a simple antibody-based electrochemical biosensor, the anti-PSA antibody was functionalized on the carbon SPE along with GO (Thunkhamrak et al., 2020) (Fig. 7(b)). When exposed to PSA antigen-spiked blood serum for detection, the immunosensor exhibited highly specific detection of the antigen. The decrease in the peak current of the probe in the voltammetric immunosensor was theoretically correlated to the PSA concentration. The obtained LOD was 270 pg mL^{-1}, while the linear range was 750 pg mL^{-1} – 100 ng mL^{-1}. In a recent effort, an electrochemical label-free immunosensor was fabricated by using a novel green synthesis approach for the quantitative detection of PSA (Darvishi et al., 2021). The detection platform was formed from quince seed mucilage containing Ag and Au NPs, which were synthesized by using green chemistry from *Calendula officinalis* L. extract. The biopolymer of quince mucilage was used to assemble the NPs to enhance the electron transfer capability. Moreover, the nanocomposite was able to increase the antibody load; hence, the sensitivity was amplified by increased electron transfer. EIS was used to detect the PSA biomarker in PSA-spiked human serum samples selectively, and the linear range was reported to be from 100 fg mL^{-1} to 100 ng mL^{-1} with a LOD of 78.0 fg mL^{-1}.

A single-stranded DNA aptamer-based biosensing platform was fabricated to detect PSA in PstC and benign prostate hyperplasia (BPH) (Aayanifard et al., 2021). The sensing platform was fabricated with GONs, which act as nanocarriers for the aptamers, and further modified with Au NPs acting as thiolated-aptamer modifiers. Herein, the authors reported a novel procedure to synthesize TiO_2/carbon QDs nanocomposite in one step and described its function as a redox probe in the electrolyte for the first time. The electroactive property, photoluminescence, and low cytotoxicity make carbon QDs suitable for

Table 7
Electrochemical detection of breast cancer biomarkers.

Analyte	EC techniques	Fabrication	LOD	Sensitivity	Range of detection	Ref.
HER2	CV, EIS, DPV	BSA/Apt/MPA/Rh-NPs/rGONs/graphite electrode	3.00 cells mL^{-1}	18.4log cells mL^{-1} cm^{-2}	5.00–10.0 × 10^4 cells mL^{-1}	Sadeghi et al. (2022)
HER2	CV, DPV	Aptamer/FGO/graphite electrode	590 pg mL^{-1}	49.5log ng mL^{-1} cm^{-2}	500 pg mL^{-1} – 25.0 ng mL^{-1}	Sadeghi et al. (2022)
CD-44	CV, EIS, DPV	BSA/anti-CD44/GO-IL-AuNPs/GCE	2.00 fg mL^{-1}	46.8 μA L $fmol^{-1}$ cm^{-2}	5.00 fg mL^{-1} – 50.0 μg mL^{-1}	Ranjan et al. (2022)
miRNA-21	CV, EIS, DPV	miRNA-21/MCH/capture DNA-21 probe/dyes-Au NPs/P3ABA/2D-MoSe2/GO-modified SPCEs	1.20 fmol L^{-1}	17.0 μA L $pmol^{-1}$ cm^{-2}	NR	Pothipor et al. (2022)
CA 15-3	CV, EIS, DPV	CA 15-3/BSA/anti-CA 15-3/dyes-Au NPs/P3ABA/2D-$MoSe_2$/GO-modified SPCEs	1.40 × 10^{-1} U mL^{-1}	17.0 μA mL U^{-1} cm^{-2}	NR	Pothipor et al. (2022)
ERBB2	CV, EIS, CA	ERBB2c/Au NPs-GO/GCE	160 pmol L^{-1}	378 nA L $nmol^{-1}$	370 pmol L^{-1} – 10.0 nmol L^{-1}	Saeed et al. (2017)
CD 24	CV, EIS, CA	CD24c/Au NPs-GO/GCE	230 pmol L^{-1}	219 nA L $nmol^{-1}$	370 pmol L^{-1} – 10.0 nmol L^{-1}	Saeed et al. (2017)

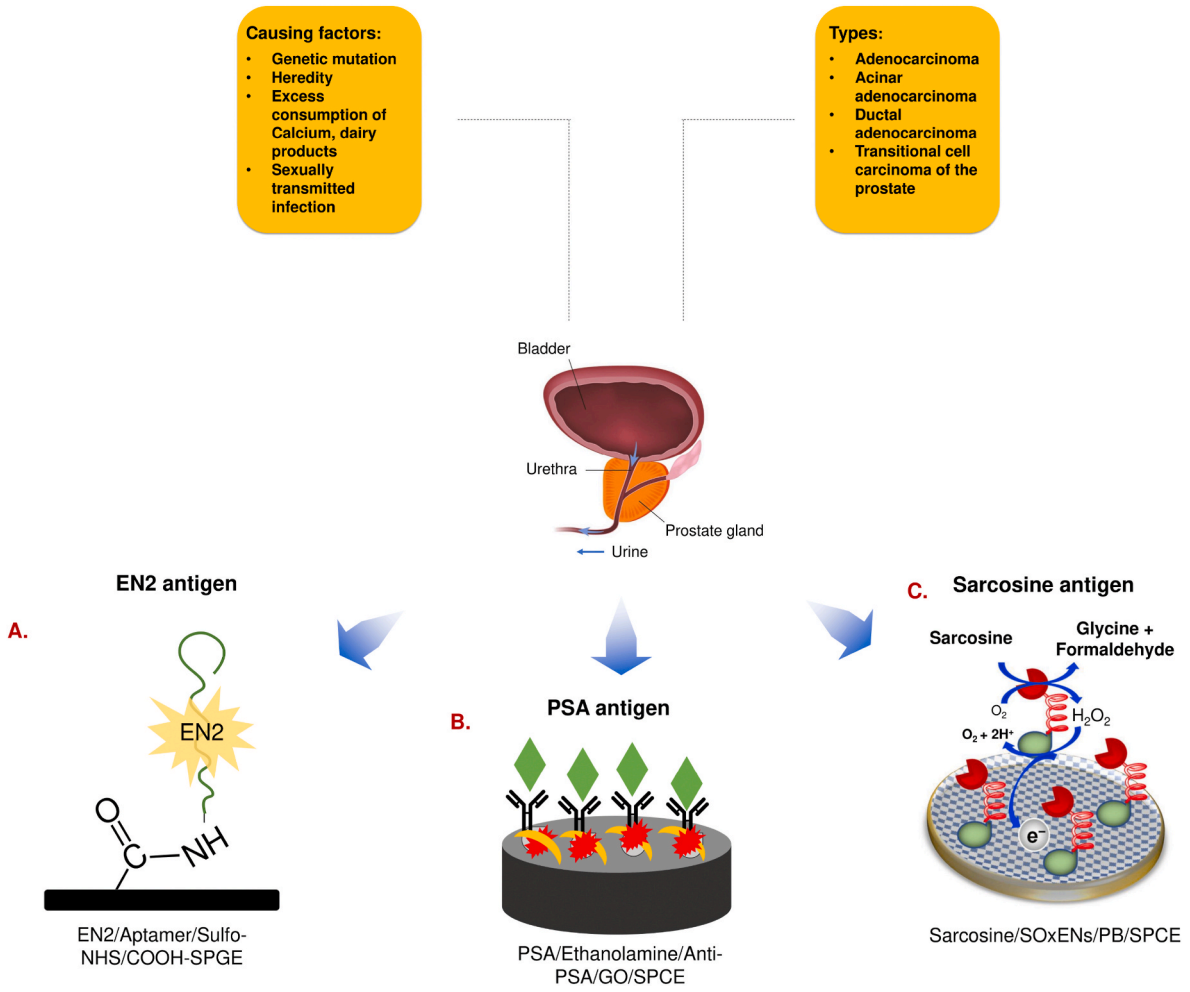

Fig. 7. Detection strategies for PstC. (a) Functionalized SPGE for the detection of EN2 antigen (reproduced with permission from Ref. (Settu et al., 2017), copyright 2017 Elsevier), (b) PSA detection by fabrication of SPCE with specific Ab (reproduced with permission from Ref. (Thunkhamrak et al., 2020), copyright 2020 Elsevier), (c) an enzyme-based sensor for the detection of sarcosine (reproduced with permission from Ref. (Niu et al., 2008), copyright 2021 Elsevier).

bioimaging and fast ion transfer in electrochemical cells. The mentioned aptamers were able to differentiate PstC from BPH based on the isoelectric pH values, which were reported and related to the irregular glycosylation process in prostate dysplastic cells. The demarcation between PstC and BPH was performed using two different pH values of 5.4 and 8.0 values, where the linear concentration of PSA was 500 pg mL^{-1} – 7.00 ng mL^{-1} and the LOD was 7.00 pg mL^{-1}. The proposed demarcation to detect the analytes at such close pH values and isoelectric pH values may impact its operating possibilities in PoC devices, where unfavorable conditions may appear, and the reliability will be limited.

Sarcosine is a metabolite present in urine that is found in significantly higher amounts in individuals suffering from PstC and correlated as a clinical biomarker for the diagnosis of PstC. Rajarathinam et al. reported the detection of sarcosine by preparing an amperometric enzymatic biosensor in spiked urine samples (Rajarathinam et al., 2021). In this work, the carbon SPE was used to fabricate the biosensor by incorporation of Prussian blue (PB) acting as the electrochemical mediator, and polymer-dispersed rGON (P-rGON) and sarcosine oxidase (SOx) were further used as enzymes (Fig. 7(c)). Here, P-rGON enhanced the electrocatalytic activity and surface area for efficient enzyme loading and rapid mass transport. The sulfonate and disulfide functional groups in poly (sodium 4-styrenesulfonate-r-LAHEMA) enabled the physical and stable absorption of SOx onto the electrode surface. The SOx converted the sarcosine to form H_2O_2, and the presence of PB enabled the quantitative detection of H_2O_2 at a low potential magnitude that correlated to sarcosine concentration.

Androgen receptors (ARs) are a part of the nuclear steroid receptor family and primarily regulate cellular differentiation in the prostate, thereby controlling growth (Niu et al., 2008). In PstC patients, the increased serological level of ARs was found to contribute to an increase in capillary diameter in tumor tissues, increasing the flow of nutrients and thus contributing to tumor growth (Lee, 2003). Increased levels of AR in body fluids are considered to be a prominent prognostic biomarker for PstC. An electrochemical aptamer-based biosensor for the selective detection of AR was prepared (Crulhas et al., 2019). The biosensing device was fabricated in a self-assembly approach using GO as a platform that was further modified with Au NPs for enhanced electrochemical activity and a thiolated-aptamer to selectively bind to AR. The prepared immunosensor employed MB as a redox label for the generation of quantifiable signal output. The researchers reported a linear detection range of 0.0–110 ng mL^{-1} for AR with a LOD of 500 pg mL^{-1}. The achieved linear range corresponds precisely with the AR values in the human prostate tissue and thus demonstrates the biosensor's ability for further integration as a diagnostic device. Table 8 shows a summary of developed electrochemical biosensors for prostate cancer detection.

4.7. Circulating tumor cells (CTCs) and circulating tumor DNA (ctDNA)

CTCs and ctNA are novel types of biomarkers that are being used for the prognosis or diagnosis of tumors. Indeed, CTCs are loose cells with tumorigenic properties in the body fluid or in the bloodstream that have been dissociated from a tumor, whereas ctDNA is derived from broken or

Table 8
Electrochemical detection of prostate cancer biomarkers.

Analyte	EC techniques	Fabrication	LOD	Sensitivity	Range of detection	Ref.
PSA	CV, EIS, DPV	PSA/anti-PSA/GO/SPCE	270 pg mL^{-1}	2.95 μA ng^{-1} mL cm^{-2}	75.0 pg mL^{-1} – 100 ng mL^{-1}	Thunkhamrak et al. (2020)
PSA	CV, EIS,	Ab-Ag/mucilage-GNPs-SNPs/GCE	78.0 fg mL^{-1}	–	100 fg mL^{-1} – 100 ng mL^{-1}	Darvishi et al. (2021)
PSA	CV, EIS, SWV	aptamer/Au NPs/GO/GCE	7.00 pg mL^{-1}	–	500 pg mL^{-1} – 7.00 ng mL^{-1}	Aayanifard et al. (2021)
Sarcosine	CV, EIS, CA	SOxENs/PB/SPCE	660 nmol L^{-1}	9.04 μA L $mmol^{-1}$ cm^{-2}	10.0–400 μmol L^{-1}	Rajarathinam et al. (2021)
AR	CV, EIS, SWV	aptamer/rGO-Au NPs/GC	50 pg mL^{-1}	NR	0.0–110 ng mL^{-1}	Crulhas et al. (2019)
EN2	CV	aptamer/SPCGE-COOH	33.8 nmol L^{-1}	NR	35.0–185 nmol L^{-1}	Settu et al. (2017)

dead tumor cells circulating in the body fluid and reflects the genome of malignant cells. Both CTCs and ctDNA can reach other tissues and transform or induce tumor formation. The utilization of CTCs and ctDNA as biomarkers to detect cancer has very recently begun.

In a simple setup, Rahimzadeh and colleagues prepared Herceptin-conjugated GO and modified GCE for the detection of breast cancer CTCs and SK-BR-3 cells in a fluid sample (Rahimzadeh et al., 2021). Herceptin is a drug molecule that utilizes a recognition domain of an antibody against HER2 and can selectively bind to breast cancer CTCs. The prepared immunosensor was tested against different cell line samples, such as MCF-7, SK-BR-3, and HUVECs, and demonstrated selective detection of SK-BR-3 cells in a linear range of 1–80 cells: the detection was simultaneously verified in human blood samples.

The detection of ctDNA from body fluid or liquid biopsy by the fabrication of DNA-based immunosensors has recently been demonstrated by different groups. In one report, Chen et al. prepared a 3D graphene-like porous multilayered carbon structure derived from the calcination of a copper-based metal nanocomposite at a very high temperature (Chen et al., 2022) (Fig. 8(a)). The platform was further loaded with Au-Pt bimetallic nanocomposite to enhance electrocatalytic activity. Detection of target ctDNA in spiked human serum samples was achieved through selective detection via capture probes on the immunosensor surface. Electrochemical measurements demonstrated accurate detection of target DNA in the presence of interfering molecules within a linear range of 10.0 nmol L^{-1} – 100 fmol L^{-1}. In another report, Guo et al. prepared a DNA-based immunosensor for the selective detection of EGFR point-mutated ctDNA (L858R) related to non-small cell lung cancer (Guo et al., 2022) (Fig. 8(b)). To fabricate immunosensors, researchers have reported the use of a Fe-based covalent organic framework. These organic frameworks have emerged as remarkable nanocomposites with highly porous structures with electronegative atoms and π bonds that are suitable for modification with biomolecules and exhibit exceptional stability. This framework was coupled with nitrogen-doped graphene material and further with Au NPs to contribute

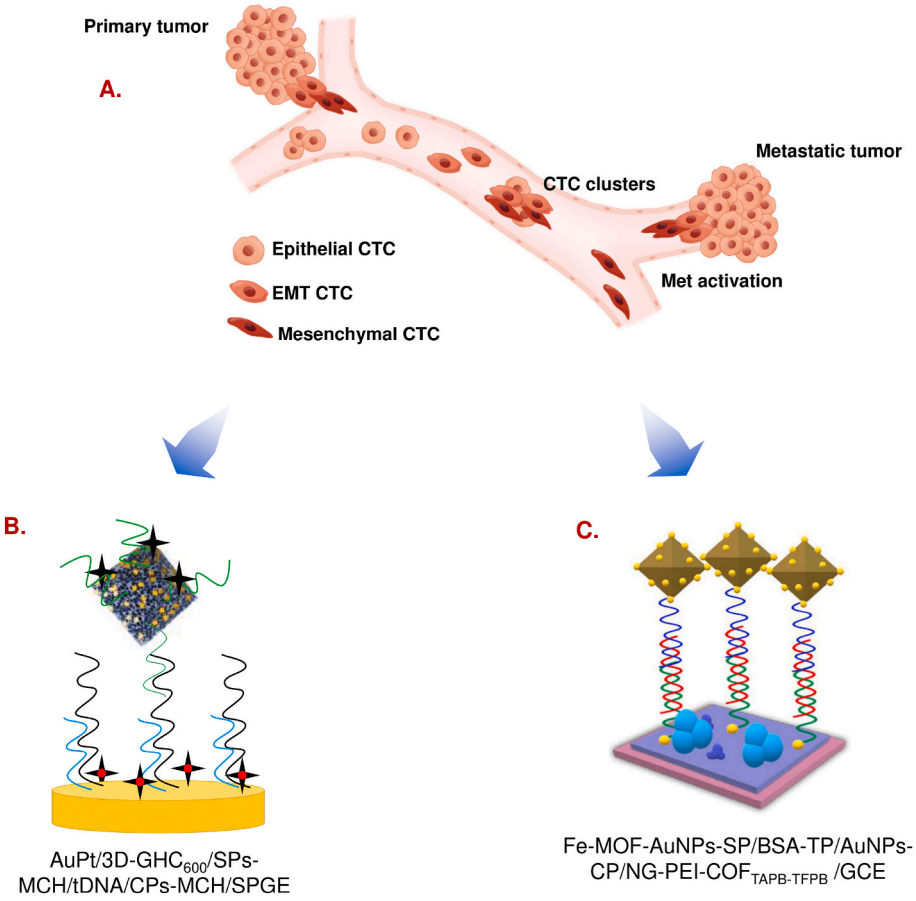

Fig. 8. Biosensing strategy for the detection of ctDNA. **(a)** Circulating tumors cells-from primary tumor to spreading through body fluid, **(b)** Fabrication of an electrochemical sensor for the detection of ctDNA (reproduced with permission from Ref. (Chen et al., 2022), copyright 2022 Elsevier), **(c)** Biosensor based on detection of ctDNA for non-small cell lung cancer (reproduced with permission from Ref. (Guo et al., 2022), copyright 2022 Elsevier).

to and amplify the electrical conductivity of the sensing platform. Additionally, PB was used in the device to generate an electrochemical signal upon the detection of target ctDNA via capture probes attached to the fabricated platform. The detection specificity and ability of the immunosensor were tested against spiked serum samples. The electrochemical performance reported ultrasensitive detection of EGFR ctDNA with the L858R mutation with excellent reproducibility with a linear detection range of 1.0 pmol L^{-1} – 100.0 nmol L^{-1}. A summary of earlier described electrochemical biosensors to detect ctDNA and CTCs is presented in Table 9.

While CTCs and ctDNA offer a promising horizon for cancer diagnosis, several disadvantages need to be considered. Firstly, both CTCs and ctDNA are present in low concentrations in the blood, making their detection challenging and potentially leading to false negatives. Secondly, the isolation and analysis of CTCs and ctDNA require sophisticated and expensive techniques, which may limit their accessibility and widespread implementation in clinical settings. Thirdly, the heterogeneity of tumors can result in variations in CTCs and ctDNA profiles, potentially leading to incomplete or inaccurate representation of the tumor's genomic landscape. Moreover, CTCs and ctDNA analysis may not be suitable for all types of cancers, as their release into the bloodstream can vary depending on tumor location and stage. Finally, ethical considerations and patient consent for the collection and analysis of blood samples containing tumor materials need to be carefully addressed. Despite these challenges, ongoing research and technological advancements aim to overcome these limitations and harness the full potential of CTCs and ctDNA for more effective and personalized cancer diagnosis and management.

5. Challenges

The application of biosensors for detecting disease biomarkers is essential in telemedicine and telemonitoring, which represent the future of healthcare. Further, the implementation of biosensors in clinical analysis results in mass screening, efficient use of expensive clinical equipment and healthcare workers, and effective therapy due to early-stage diagnosis. However, to be globally practiced, biosensing in general and biosensors-based on graphene-based materials must overcome several issues that prevent academic research from being commercialized.

Graphene-based electrochemical biosensors have demonstrated true potential to be incorporated into real-time diagnostics as a general practice. The works discussed in this review present a variety of efficient fabrication strategies to prepare biosensors for the selective and rapid detection of cancer biomarkers. On the other hand, nanomaterial-modified biosensors also face a few challenges. The function of graphene derivatives in a biosensor is crucial to enhance electrical conductivity and to provide a large modifiable surface area suitable for the immobilization of bio-receptors. Therefore, the efficiency and reproducibility of detection are partially dependent on the quality and purity of the nanomaterials. The physicochemical properties and surface functionalities of graphene-based nanomaterials depend on the uniform synthesis route and oxidation/reduction methods. Physical factors of carbon-based nanomaterials, such as lateral size, number of immobilized layers, and purity of graphene nanomaterials, also play crucial roles in determining the efficiency of the biosensor. The number of bio-receptors loaded onto the modified surface based on physical properties determines the sensitivity and amplification of the output signal. Future studies must focus on the homogenization of the fabrication process to significantly improve intra- and inter-electrode reproducibility. In other words, a significant difference in the number of bio-receptors immobilized on the surface can produce varied amounts of output signals, thereby decreasing the reproducibility. Further research is required to achieve near-identical physiochemical properties of the sensing platform to enhance efficiency.

The sensitivity and selectivity in the detection of biomarkers by using the biosensors rely on the bioreceptors. The most widely used bioreceptors, such as antibodies, are costly due to their sophisticated synthesis process and storage conditions. Moreover, as in the case of monoclonal antibodies that are more specific to target antigens, sometimes the purification affects the sensitivity (Jain et al., 2021). Furthermore, the poor stability of biomolecules in operating conditions limits the shelf-life of the produced biosensors (Mukherjee et al., 2023; Ashrafi et al., 2021). Nevertheless, lately, the application of aptamers designed for various biomarkers seems to be an efficient approach to substitute for antibodies. Even though the generation of aptamers is a tedious and sophisticated process, however, the progress in the SELEX strategies (modern aptamer generation process) has improved this process (Byakodi et al., 2022). Indeed, to commercialize the biosensor for application in clinical applications, an enormous number of control tests must be performed to fully validate the results and ensure reproducibility, precision, and accuracy. Only after this, the end user can trust the PoC devices. This requires a large amount of the purified biomolecule from a biological source (Teles et al., 2010).

An additional difficulty in biosensor development is finding an effective way to attach the bioreceptors to the transducer surface without compromising their affinity for the target compound. This can be complicated by factors such as interactions with other compounds, presence in the transducer matrix, and incorrect orientation on the surface (Li et al., 2020; Meng et al., 2023). One major restriction in the practical use of biosensors is the likelihood of interfering compounds in complex biological fluids such as blood, serum, urine, or saliva (Senf et al., 2020). Herein, the pretreatment steps are required to get rid of the interfering agents that consequently impair the simplicity required in PoC analysis by an untrained end user. Similarly, sometimes even the sample collection must be performed by skilled personnel which is another obstacle to the PoC analysis. Therefore, all these factors that necessitate the pre-analytical, analytical, and post-analytical processing, limit their application by the untrained users as they are not sufficiently equipped to perform equal quality control of the tests. To address this, the researchers are working on microfluidics systems which are multifunctional devices capable of running an analytical assay with the necessary pretreatment, and amplification. However, the research in this field is still in its infancy as there are challenges in terms of implementation and clinical validation (Choi et al., 2011).

In addition, portability is a significant character of the biosensors to be applied in PoC analysis, requiring miniaturization as an essential mission. It demands further advancements in microelectronics, and the electrical circuit dimensions to fabricate miniaturized PoC platforms. The last but not the least, the disposable nature of biosensors as PoC

Table 9
Electrochemical detection of ctDNA and circulating cells in published literature.

Analyte	EC techniques	Fabrication	LOD	Sensitivity	Range of detection	Ref.
Breast cancer SK-BR-3 cell	CV, EIS, SWV	Herceptin-20 cells/Im-graphene/GCE	–	NR	1.00–80.0 cells	Rahimzadeh et al. (2021)
ctDNA	CA, EIS, CV	SPs-label/tDNA/MCH/CPs/SPGE	2.25×10^{-8} mol L^{-1}	NR	1.00×10^{-8} – 1.00×10^{-17} mol L^{-1}	Chen et al. (2022)
EGFR (L858R)	CV, DPV, EIS	TP/BSA/CP/Au NPs/NG-PEI-$COF_{TAPB-TFPB}$/GCE.	7.65 fmol L^{-1}	NR	100 fmol L^{-1} – 100 nmol L^{-1}	Guo et al. (2022)

devices may be problematic in terms of resources and the final cost, particularly in regions with limited resources.

In a more general sense, the detection of a specific cancer type targeting a biomarker faces a challenge in terms of specificity. On the one hand, many biomarkers are reported to be linked to different types of cancers, while on the other hand, many benign tumor conditions also exhibit similar clinical values of certain biomarkers, which often creates a misconception about malignancy. Biosensors are effective devices as a starting point for regular monitoring to obtain a hint of underlying physiological conditions via a rapid, time-saving, low-cost test with minimal labor. However, due to the limitation regarding the specificity of a biomarker, the clinical correlation to malignancy should be drawn after further conventional diagnosis. Therefore, the devised biosensors can be used for preliminary analysis among people who are likely to have cancer diseases due to their work environment, genetic inheritance, and lifestyle. Thereafter, those who are diagnosed with suspicion of cancer can be directed to more expensive, time-consuming, and sophisticated conventional diagnosis methods.

6. Future perspectives

The key to the effective management of cancer and control of metastasis greatly relies on innovative, early, and effective diagnosis. Decades of research and development have improved the understanding of interactions between biological macromolecules and inorganic materials. By harnessing the knowledge of biochemical interactions and electrochemistry, electrochemical biosensors serve as ideal solutions for becoming frontrunners in the new generation of medical biology and improved diagnostics. An ideal electrochemical biosensor must exhibit a) high sensitivity, b) a simpler fabrication strategy and efficient long-term storage, c) minimal sample requirements, d) the ability to process a large number of samples in minimal time with less labor, e) a high reproducibility, and f) an electrochemical platform that should enable miniaturization for PoC applications.

The focus of new-age biosensing platforms is manifesting increasingly user-friendly PoC biosensors that offer fast and reliable detection through small devices allowing easy mobility. The integration of the modern concepts such as the Internet of Medical Things (IoMT) and Artificial Intelligence (AI) holds tremendous potential for revolutionizing early cancer detection using electrochemical biosensors. As cancer remains one of the leading causes of mortality worldwide, there is an urgent need for advanced and efficient diagnostic tools to enable early detection and personalized treatment. Electrochemical biosensors, capable of detecting specific cancer biomarkers with high sensitivity, have shown promise in this regard. By coupling these biosensors with IoMT, a network of interconnected medical devices and applications, real-time data transmission and monitoring become possible. This connectivity facilitates seamless communication between biosensors and storage servers, enabling continuous monitoring of cancer biomarkers in patients. AI algorithms can analyze vast and complex data from sensors and detect patterns, trends, and correlations through machine learning-trained neural networks that may be imperceptible to human observation. The ability of AI to process large datasets quickly and accurately allows for the detection of subtle and rapid changes in biomarker levels, which could indicate early-stage cancer or disease progression. This early detection is crucial, as it may lead to timely interventions, improving patient outcomes and survival rates. Moreover, AI's capacity for machine learning enables the continuous improvement of its analysis capabilities over time, leading to refined and more accurate cancer detection algorithms. By incorporating patient-specific data, such as genetic profiles and medical history, AI can support the development of personalized cancer detection and treatment plans, tailoring approaches to each patient's unique characteristics. Additionally, the combination of IoMT and AI facilitates remote and point-of-care monitoring, enabling healthcare providers to access real-time data from patients regardless of their location. This feature is particularly valuable for patients in remote areas or those undergoing home-based care. The use of AI-driven data analytics provides healthcare professionals with valuable support, aiding them in interpreting complex datasets generated by the biosensors. The AI algorithms can help identify critical biomarker fluctuations and provide alerts for timely interventions. Furthermore, the integration of IoMT and AI with electrochemical biosensors opens avenues for research and innovation, as the continuous feedback loop allows for iterative improvements and advancements in the field of cancer diagnostics. In conclusion, the synergistic collaboration of IoMT and AI with electrochemical biosensors has the potential to transform cancer diagnostics by enabling real-time monitoring, early detection, personalized medicine, and data-driven decision support. This convergence represents a paradigm shift in cancer care, empowering healthcare professionals with enhanced diagnostic capabilities and, ultimately, contributing to improved patient outcomes and quality of life.

Indeed, new technologies in biosensors for disease biomarkers should be directed toward micro-/nano-fabrication to achieve the miniaturization needed for the portability and incorporation of AI concepts. With this regard, the main efforts are focused on the incorporation of electrical and micro-electrical advancement into the biosensing platform to use the unique features demanded in the healthcare system. For an instance, IoMT offers wireless operation, and communication service that promotes the automation of PoC biosensing platforms by facilitating data collection and transmission through satellite networks (Jain et al., 2021). Additionally, the market availability of the small-sized portable electrochemical analyzers enables the miniaturization of electrochemical biosensors. The advancement in technology promotes the miniaturization and portability of the biosensors. To this end, electronic products such as smartphones, and Bluetooth connectivity can be employed in measurement, data collection, and transmission. A graphical user interface (GUI) in smartphones can function as an electrochemical analyzer that can easily connect with screen-printed electrodes, resembling a lab-on-a-chip approach. Herein the digitalized devices can contribute to the cutting-edge automated services needed for the PoC analysis by the biosensors. On the other hand, web browsers and servers can also offer an interface for transferring, and storing receiving health information in real-time (represented in Fig. 9).

The consumption of energy in implantable and wearable biosensors is an important concept for continuous monitoring over long periods. Therefore, new approaches in this regard have evolved such as triboelectric nanogenerators that allow efficient conversion (85 %) of the in vivo biological and mechanical energy generated by body movements such as breathing, heart beating, blood flow, muscle stretching, lung vibration, to the required electrical energy of the biosensor and storage for the further use (Solanki et al., 2023).

Moreover, the integration of the biosensing platform into a cloud-based system leads to a powerful framework enabling multistep assay (sample preparation, pretreatment, and amplified detection) that suits PoC analysis in the field in real-time. Therefore, portable microfluidics systems connected to application-based GUI and data storage servers can be fascinating for researchers to design a platform capable of performing all the necessary analytical steps.

CRediT authorship contribution statement

Soumajit Mukherjee: Formal analysis, Visualization, Writing – original draft. **Atripan Mukherjee:** Formal analysis, Methodology, Validation. **Zuzana Bytesnikova:** Conceptualization, Investigation, Methodology, Validation. **Amir M. Ashrafi:** Conceptualization, Data curation, Writing – original draft. **Lukas Richtera:** Investigation, Supervision, Validation, Visualization, Writing – review & editing. **Vojtech Adam:** Conceptualization, Funding acquisition, Project administration, Writing – review & editing.

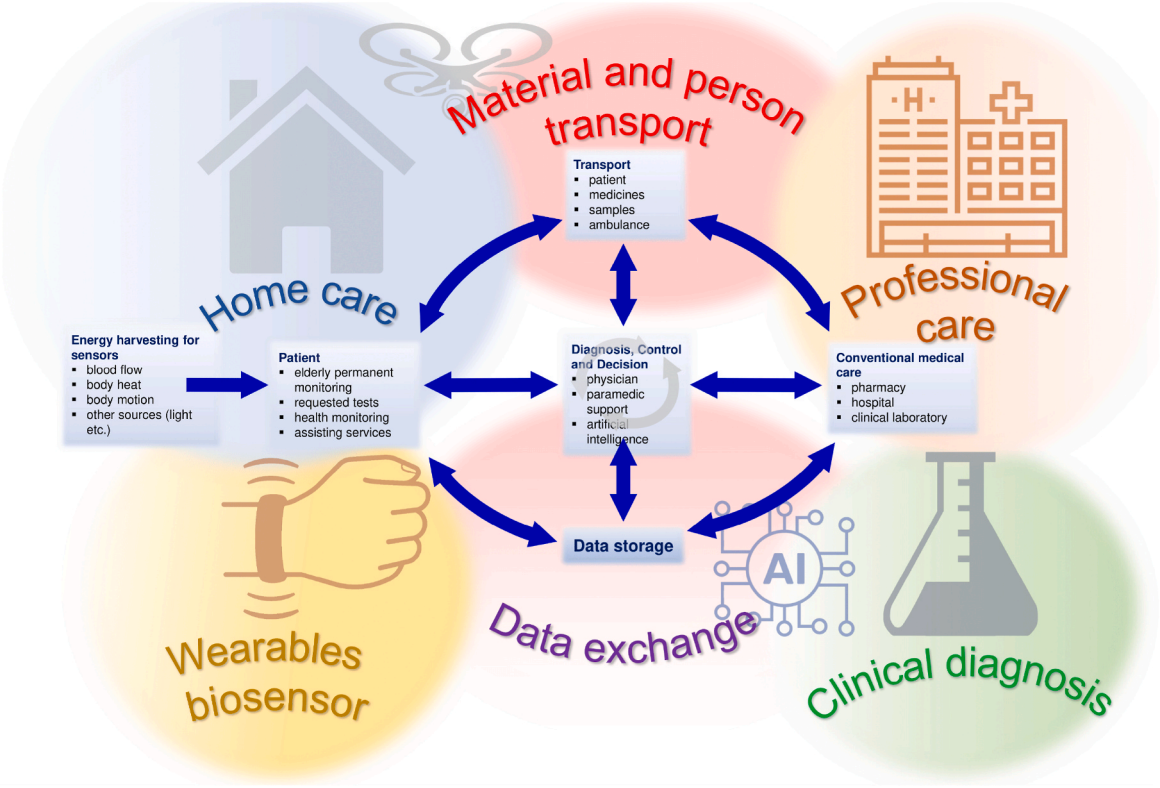

Fig. 9. Futuristic concept for the effeicient integration of smart wearable biosensors into AI-assisted diagnosis to promote immediate and at-home care.

Declaration of competing interest

The authors declare that they have no known competing financial interests or personal relationships that could have appeared to influence the work reported in this paper.

Data availability

No data was used for the research described in the article.

Acknowledgments

This work was supported by the ERFD "Multidisciplinary research to increase application potential of nanomaterials in agricultural practice" No. CZ.02.1.01/0.0/0.0/16_025/0007314.

List of abbreviations

Ab	Antibody
AFP	Alpha-fetoprotein
APC	Adenomatous polyposis coli
AR	Androgen receptor
BAX	Bcl-2-associated X protein
Bcl2	B-cell lymphoma 2
CA 19-9	Carbohydrate antigen 19-9
CA 72-4	Carbohydrate antigen 72-4
CD-44	Cluster of differentiation-44
CEA	Carcinoembryonic antigen
ctDNA	Circulating tumor DNA
EGFR	Epidermal growth factor receptor
EN2	Engrailed homeobox 2
EpCAMs	Epithelial cell adhesion molecules
GO	Graphene oxide
HER2	Human epidermal growth factor receptor 2
IL-8	Interleukin 8
KIT	KIT proto-oncogene
LDH	Lactate dehydrogenase
miR-21	microRNA-21
MMP-7	Matrix metalloproteinase 7
Muc-1	Mucin 1
NSE	Neuron-specific enolase
p53	Tumor protein 53 x
ORAOV1	Oral cancer overexpressed 1
PEAK-1	Pseudopodium enriched atypical kinase 1
PSA	Prostate-specific antigen
SPE	Screen-printed electrode
QDs	Quantum dots
PoC	Point-of-Care
rGO	reduced graphene oxide
CV	Cyclic Voltammetry
EIS	Electrochemical Impedance Spectroscopy
DPV	Differential Pulse Voltammetry
CA	Chronoamperometry
SWV	Square Wave Voltammetry
LSV	Linear Sweep Voltammetry
NR	sensitivity calculation was not possible because the surface area of the used electrode was not reported

References

Aayanifard, Z., Alebrahim, T., Pourmadadi, M., Yazdian, F., Dinani, H.S., Rashedi, H., Omidi, M., 2021. Eng. Life Sci. 21, 739–752.
Agarwal, V., Zetterlund, P.B., 2021. Chem. Eng. J. 405, 29.
Akbari, A., Hashemzadeh, H., Eshkiki, Z.S., Masoodi, M., Tabaeian, S.P., Naderi-Manesh, H., Zare, A.A., Agah, S., 2023. Biosens. Bioelectron. X 14, 100331.
Akdis, M., 2011. J. Allergy Clin. Immunol. 128, 739-739.
Alava, T., Mann, J.A., Theodore, C., Benitez, J.J., Dichtel, W.R., Parpia, J.M., Craighead, H.G., 2013. Anal. Chem. 85, 2754–2759.
Ambrosi, A., Pumera, M., 2014. Nanoscale 6, 472–476.
Arya, S.K., Wang, K.Y., Wong, C.C., Rahman, A.R.A., 2013. Biosens. Bioelectron. 41, 446–451.

Ashrafi, A.M., Bytesnikova, Z., Barek, J., Richtera, L., Adam, V., 2021. Biosens. Bioelectron. 192, 18.
Aydın, E.B., Aydın, M., Sezgintürk, M.K., 2020. Sensor. Actuator. B Chem. 306, 127613.
Aydin, E.B., Aydin, M., Sezginturk, M.K., 2023. Sens. Actuator B-Chem. 378, 11.
Babaei, K., Shams, S., Keymoradzadeh, A., Vahidi, S., Hamami, P., Khaksar, R., Norollahi, S.E., Samadani, A.A., 2020. Life Sci. 240, 1–13.
Balaji, A., Zhang, J., 2017. Cancer Nanotechnol 8, 10.
Bellardita, M., Garcia-Lopez, E.I., Marci, G., Krivtsov, I., Garcia, J.R., Palmisano, L., 2018. Appl. Catal. B Environ. 220, 222–233.
Bonanni, A., Loo, A.H., Pumera, M., 2012. Trac. Trends Anal. Chem. 37, 12–21.
Byakodi, M., Shrikrishna, N.S., Sharma, R., Bhansali, S., Mishra, Y., Kaushik, A., Gandhi, S., 2022. Biosens. Bioelectron. X 12, 100284.
Carraro, G., Savio, L., Vattuone, L., 2022. Coatings 12, 19.
Castelletto, S., Boretti, A., 2021. RSC Adv. 11, 7981–8002.
Cervino, G., Fiorillo, L., Herford, A.S., Romeo, U., Bianchi, A., Crimi, S., D'Amico, C., De Stefano, R., Troiano, G., Santoro, R., Laino, L., Laino, G., Cicciu, M., 2019. Dis. Markers 2019, 1–11.
Chatterjee, S.K., Zetter, B.R., 2005. Future Oncol. 1, 37–50.
Chen, W.Y., Rosner, B., Hankinson, S.E., Colditz, G.A., Willett, W.C., 2011. JAMA, J. Am. Med. Assoc. 306, 1884–1890.
Chen, G.Y., Pang, D.W.P., Hwang, S.M., Tuan, H.Y., Hu, Y.C., 2012. Biomaterials 33, 418–427.
Chen, J.Y., Tsai, W.S., Shao, H.J., Wu, J.C., Lai, J.M., Lu, S.H., Hung, T.F., Yang, C.T., Wu, L.C., Chen, J.S., Lee, W.H., Chang, Y.C., 2016. PLoS One 11, 1–21.
Chen, C., Sun, W., Lv, H.Y., Li, H., Wang, Y.B., Wang, P., 2018. Chem. Eng. J. 350, 949–959.
Chen, K.C., Zhao, H.L., Wang, Z.X., Lan, M.B., 2022. Mater. Today Chem. 24, 100892.
Cheng, Q.Y., Han, B.H., 2013. J. Nanosci. Nanotechnol. 13, 755–760.
Cheng, G., Zhang, J.L., Liu, Y.L., Sun, D.H., Ni, J.Z., 2011. Chem. Commun. 47, 5732–5734.
Cho, H.S., Mason, K., Ramyar, K.X., Stanley, A.M., Gabelli, S.B., Denney, D.W., Leahy, D. J., 2003. Nature 421, 756–760.
Choi, S., Goryll, M., Sin, L.Y.M., Wong, P.K., Chae, J., 2011. Microfluid. Nanofluidics 10, 231–247.
Crulhas, B.P., Basso, C.R., Parra, J., Castro, G.R., Pedrosa, V.A., 2019. J. Sens. 2019, 1–11.
Cuk, K., Zucknick, M., Heil, J., Madhavan, D., Schott, S., Turchinovich, A., Arlt, D., Rath, M., Sohn, C., Benner, A., Junkermann, H., Schneeweiss, A., Burwinkel, B., 2013. Int. J. Cancer 132, 1602–1612.
Darvishi, E., Ehzari, H., Shahlaei, M., Behbood, L., Arkan, E., 2021. Bioelectrochemistry 139, 107744.
Das, M., Dhand, C., Sumana, G., Srivastava, A.K., Vijayan, N., Nagarajan, R., Malhotra, B. D., 2011. Appl. Phys. Lett. 99, 1–3.
Dreyer, D.R., Park, S., Bielawski, C.W., Ruoff, R.S., 2010. Chem. Soc. Rev. 39, 228–240.
Du, D., Yan, F., Liu, S.L., Ju, H.X., 2003. J. Immunol. Methods 283, 67–75.
Du, X., Zheng, X.D., Zhang, Z.H., Wu, X.F., Sun, L., Zhou, J., Liu, M., 2019. Nanomaterials 9, 1–12.
Durovic, A., Stojanovic, Z., Bytesnikova, Z., Kravic, S., Svec, P., Pribyl, J., Richtera, L., 2022. J. Mater. Sci. 57, 5533–5551.
Fang, Y., Li, Y., Zhang, M., Cui, B., Hu, Q., Wang, L., 2019. Analyst 144, 2186–2194.
Fernandez-Merino, M.J., Guardia, L., Paredes, J.I., Villar-Rodil, S., Solis-Fernandez, P., Martinez-Alonso, A., Tascon, J.M.D., 2010. J. Phys. Chem. C 114, 6426–6432.
Fitzgibbons, P.L., Page, D.L., Weaver, D., Thor, A.D., Allred, C., Clark, G.M., Ruby, S.C., O'Malley, F., Sinpson, L.F., Connolly, J.L., Hayes, D.F., Edge, S.B., Lichter, A., Schnitt, S.J., 2000. Arch. Pathol. Lab Med. 124, 966–978.
Fu, S., Ning, Z., Li, Q., He, Y., Xie, C., Cheng, J., Ye, H., Li, Q., Jaffrezic-Renault, N., Feng, J., Guo, Z., 2023. Sensor. Actuator. B Chem. 392, 134086.
Ganganboina, A.B., Doong, R.A., 2019. Sci. Rep. 9, 1–11.
Gao, Y., Kyratzis, I., 2008. Bioconjugate Chem. 19, 1945–1950.
Geim, A.K., Novoselov, K.S., 2007. Nat. Mater. 6, 183–191.
Geim, A.K., Novoselov, K.S., 2010. The rise of graphene. In: Nanoscience and Technology: a Collection of Reviews from Nature Journals. World Scientific, pp. 11–19.
Gogoi, D., Makkar, P., Ghosh, N.N., 2021. ACS Omega 6, 4831–4841.
Goh, M.S., Pumera, M., 2010a. Chem. Asian J. 5, 2355–2357.
Goh, M.S., Pumera, M., 2010b. Electrochem. Commun. 12, 1375–1377.
Gomez-Navarro, C., Burghard, M., Kern, K., 2008. Nano Lett. 8, 2045–2049.
Goutsouliak, K., Veeraraghavan, J., Sethunath, V., De Angelis, C., Osborne, C.K., Rimawi, M.F., Schiff, R., 2020. Nat. Rev. Clin. Oncol. 17, 233–250.
Guo, F., Creighton, M., Chen, Y.T., Hurt, R., Kulaots, I., 2014. Carbon 66, 476–484.
Guo, L., Mu, Z., Yan, B., Wang, J., Zhou, J., Bai, L., 2022. Sensor. Actuator. B Chem. 350, 130874.
Haglund, C., Lundin, J., Kuusela, P., Roberts, P.J., 1994. Br. J. Cancer 70, 487–492.
Han, C., Zhang, N., Xu, Y.J., 2016. Nano Today 11, 351–372.
Hartati, Y.W., Letelay, L.K., Gaffar, S., Wyantuti, S., Bahti, H.H., 2020. Sens. Bio-Sens. Res 27, 1–8.
Henderson, T.O., Amsterdam, A., Bhatia, S., Hudson, M.M., Meadows, A.T., Neglia, J.P., Diller, L.R., Constine, L.S., Smith, R.A., Mahoney, M.C., Morris, E.A., Montgomery, L. L., Landier, W., Smith, S.M., Robison, L.L., Oeffinger, K.C., 2010. Ann. Intern. Med. 152, 444-W154.
Henry, N.L., Hayes, D.F., 2012. Mol. Oncol. 6, 140–146.
Hernandez, J., Thompson, I.M., 2004. Cancer 101, 894–904.
Hernandez-Cancel, G., Suazo-Davila, D., Ojeda-Cruzado, A.J., Garcia-Torres, D., Cabrera, C.R., Griebenow, K., 2015. J. Nanobiotechnol. 13, 12.
Hofer, C., Skakalova, V., Gorlich, T., Tripathi, M., Mittelberger, A., Mangler, C., Monazam, M.R.A., Susi, T., Kotakoski, J., Meyer, J.C., 2019. Nat. Commun. 10, 8.
Holzinger, M., Le Goff, A., Cosnier, S., 2014. Front. Chem. 2, 10.
Hou, C., Wang, Y., Zhu, H., Wei, H., 2016. Chem. Eng. J. 283, 397–403.
Iannazzo, D., Espro, C., Celesti, C., Ferlazzo, A., and Neri, G. (2021) 13, 3194..
Ibáñez-Redín, G., Furuta, R.H.M., Wilson, D., Shimizu, F.M., Materon, E.M., Arantes, L. M.R.B., Melendez, M.E., Carvalho, A.L., Reis, R.M., Chaur, M.N., Gonçalves, D., Oliveira Jr., O.N., 2019. Mater. Sci. Eng. C 99, 1502–1508.
Isbell, J.M., Jones, D.R., Li, B.T., 2018. J. Thorac. Cardiovasc. Surg. 155, 2628–2631.
Jafari-Kashi, A., Rafiee-Pour, H.-A., Shabani-Nooshabadi, M., 2022. Chemosphere 301, 134636.
Jain, S., Nehra, M., Kumar, R., Dilbaghi, N., Hu, T.Y., Kumar, S., Kaushik, A., Li, C.Z., 2021. Biosens. Bioelectron. 179, 26.
Jalil, O., Pandey, C.M., Kumar, D., 2020. Microchim. Acta 187, 1–9.
Janegitz, B.C., Silva, T.A., Wong, A., Ribovski, L., Vicentini, F.C., Taboada Sotomayor, M. d.P., Fatibello-Filho, O., 2017. Biosens. Bioelectron. 89, 224–233.
Jin, L.L., Yang, K., Yao, K., Zhang, S., Tao, H.Q., Lee, S.T., Liu, Z., Peng, R., 2012. ACS Nano 6, 4864–4875.
Jin, B., Wang, P., Mao, H., Hu, B., Zhang, H., Cheng, Z., Wu, Z., Bian, X., Jia, C., Jing, F., Jin, Q., Zhao, J., 2014. Biosens. Bioelectron. 55, 464–469.
Joshi, S., Raj, K.A., Rao, M.R., Ghosh, R., 2022. Sci. Rep. 12, 3006.
Kang, X.H., Wang, J., Wu, H., Liu, J., Aksay, I.A., Lin, Y.H., 2010. Talanta 81, 754–759.
Kashyap, D., Kaur, H., 2020. Life Sci. 246, 1–13.
Keller, L., Werner, S., Pantel, K., 2019. Cell Stress 3, 165–180.
Kelsey, J.L., Gammon, M.D., John, E.M., 1993. Epidemiol. Rev. 15, 36–47.
Khatri, R., Puri, N.K., 2022. J. Mater. Res. 37, 1451–1463.
Kim, H., Namgung, R., Singha, K., Oh, I.K., Kim, W.J., 2011. Bioconjugate Chem. 22, 2558–2567.
Kim, J., Park, S.J., Min, D.H., 2017. Anal. Chem. 89, 232–248.
King, M.C., Marks, J.H., Mandell, J.B., New York Breast Canc Study, G., 2003. Science 302, 643–646.
Kou, B.B., Zhang, L., Xie, H., Wang, D., Yuan, Y.L., Chai, Y.Q., Yuan, R., 2016. ACS Appl. Mater. Interfaces 8, 22869–22874.
Kumar, S., Sharma, J.G., Maji, S., Malhotra, B.D., 2016. Biosens. Bioelectron. 78, 497–504.
Kumar, S., Panwar, S., Kumar, S., Augustine, S., Malhotra, B.D., 2019. Nanomaterials 9, 1–14.
Labib, M., Sargent, E.H., Kelley, S.O., 2016. Chem. Rev. 116, 9001–9090.
Lahmann, P.H., Hoffmann, K., Allen, N., Van Gils, C.H., Khaw, K.T., Tehard, B., Berrino, F., Tjonneland, A., Bigaard, J., Olsen, A., Overvad, K., Clavel-Chapelon, F., Nagel, G., Boeing, H., Trichopoulos, D., Economou, G., Bellos, G., Palli, D., Tumino, R., Panico, S., Amiano, P., Pera, G., Quiros, J.R., Martinez, C., Tormo, M.J., Wirfalt, E., Berglund, G., Hallmans, G., Key, T.J., Reeves, G., Bingham, S., Norat, T., Biessy, C., Kaaks, R., Riboli, E., 2004. Int. J. Cancer 111, 762–771.
Lai, C.H., Lim, S.C., Wu, L.C., Wang, C.F., Tsai, W.S., Wu, H.C., Chang, Y.C., 2017. Chem. Commun. 53, 4152–4155.
Lee, D., 2003. Clin. Prostate. Cancer 2, 13–14.
Lee, C., Wei, X.D., Kysar, J.W., Hone, J., 2008. Science 321, 385–388.
Li, Y.J., Feng, L.Z., Shi, X.Z., Wang, X.J., Yang, Y.L., Yang, K., Liu, T., Yang, G.B., Liu, Z., 2014. Small 10, 1544–1554.
Li, N.D., Wang, Y.C., Liu, X.F., Luo, P., Jing, W., Zhu, M., Tu, J.C., 2017. Technol. Cancer Res. Treat. 16, 1060–1066.
Li, S.H., Zhang, N., Xie, X.Q., Luque, R., Xu, Y.J., 2018. Angew. Chem.-Int. Edit. 57, 13082–13085.
Li, J.Y., Liu, J.J., Bi, Y.N., Sun, M.M., Bai, J., Zhou, M., 2020. Anal. Chim. Acta 1105, 87–94.
Li, L., Wang, S. Y., Xiao, Y., and Wang, Y. (2020) Transactions Tianjin Univ. 26, 424-440..
Liang, Z.X., Ou, D., Sun, D.P., Tong, Y.L., Luo, H.B., Chen, Z.G., 2019. Biosens. Bioelectron. 146, 8.
Lim, S., Park, H., Yamamoto, G., Lee, C., Suk, J.W., 2021. Nanomaterials 11, 12.
Liu, G.D., Lin, Y.H., 2005. Anal. Chem. 77, 5894–5901.
Lu, K.Q., Li, Y.H., Zhang, F., Qi, M.Y., Chen, X., Tang, Z.R., Yamada, Y.M.A., Anpo, M., Conte, M., Xu, Y.J., 2020. Nat. Commun. 11, 9.
Meng, X., O'Hare, D., Ladame, S., 2023. Biosens. Bioelectron. 237, 115440.
Miao, W., Shim, G., Kang, C.M., Lee, S., Choe, Y.S., Choi, H.G., Oh, Y.K., 2013. Biomaterials 34, 9638–9647.
Mitchell, P.S., Parkin, R.K., Kroh, E.M., Fritz, B.R., Wyman, S.K., Pogosova-Agadjanyan, E.L., Peterson, A., Noteboom, J., O'Briant, K.C., Allen, A., Lin, D.W., Urban, N., Drescher, C.W., Knudsen, B.S., Stirewalt, D.L., Gentleman, R., Vessella, R. L., Nelson, P.S., Martin, D.B., Tewari, M., 2008. Proc. Natl. Acad. Sci. U. S. A 105, 10513–10518.
Mo, F.J., Chen, M., Meng, H., Wu, J.L., Fu, Y.Z., 2020. Sens. Actuator B-Chem. 309.
Monteiro, M., Moreira, N., Pinto, J., Pires-Luis, A.S., Henrique, R., Jeronimo, C., Bastos, M.D., Gil, A.M., Carvalho, M., de Pinho, P.G., 2017. J. Cell Mol. Med. 21, 2092–2105.
Mukherjee, A., Ashrafi, A.M., Bytesnikova, Z., Svec, P., Richtera, L., Adam, V., 2023. J. Electroanal. Chem. 935, 11.
Murata, H., Nakajima, Y., Saitoh, N., Yoshizawa, N., Suemasu, T., Toko, K., 2019. Sci. Rep. 9, 5.
Niu, Y., Altuwaijri, S., Lai, K.-P., Wu, C.-T., Ricke, W.A., Messing, E.M., Yao, J., Yeh, S., Chang, C., 2008. Proc. Natl. Acad. Sci. USA. 105, 12182–12187.
Ordonez, N.G., 2014. Appl. Immunohistochem. 22, 331–347.
Ortega, F.G., Fernandez-Baldo, M.A., Serrano, M.J., Messina, G.A., Lorente, J.A., Raba, J., 2015. Sens. Actuator B-Chem. 221, 248–256.
Pachauri, N., Dave, K., Dinda, A., Solanki, P.R., 2018. J. Mater. Chem. B 6, 3000–3012.
Paimard, G., Shahlaei, M., Moradipour, P., Akbari, H., Jafari, M., Arkan, E., 2020. Sens. Actuator B-Chem. 311, 1–10.

Palomar, Q., Xu, X.X., Selegard, R., Aili, D., Zhang, Z., 2020. Sens. Actuator B-Chem. 325, 8.
Pandha, H., Sorensen, K.D., Orntoft, T.F., Langley, S., Hoyer, S., Borre, M., Morgan, R., 2012. BJU Int. 110, E287–E292.
Papageorgiou, D.G., Kinloch, I.A., Young, R.J., 2017. Prog. Mater. Sci. 90, 75–127.
Paranthaman, V., Sundaramoorthy, K., Chandra, B., Muthu, S.P., Alagarsamy, P., Perumalsamy, R., 2018. Phys. Status Solidi A-Appl. Mat. 215, 9.
Park, S., Ruoff, R.S., 2009. Nat. Nanotechnol. 4, 217–224.
Park, S., Mohanty, N., Suk, J.W., Nagaraja, A., An, J.H., Piner, R.D., Cai, W.W., Dreyer, D. R., Berry, V., Ruoff, R.S., 2010. Adv. Mater. 22, 1736–+.
Pattammattel, A., Puglia, M., Chakraborty, S., Deshapriya, I.K., Dutta, P.K., Kumar, C.V., 2013. Langmuir 29, 15643–15654.
Pavanello, S., Clonfero, E., 2000. Mutat. Res. Rev. Mutat. Res. 463, 285–308.
Pei, S., Cheng, H.-M., 2012. Carbon 50, 3210–3228.
Pei, S.F., Zhao, J.P., Du, J.H., Ren, W.C., Cheng, H.M., 2010. Carbon 48, 4466–4474.
Peña-Bahamonde, J., Nguyen, H.N., Fanourakis, S.K., Rodrigues, D.F., 2018. J. Nanobiotechnol. 16, 75.
Perkins, G.L., Slater, E.D., Sanders, G.K., Prichard, J.G., 2003. Am. Fam. Physician 68, 1075–1082.
Porcel, J.M., Esquerda, A., Bielsa, S., Novell, A., Sorolla, M.A., Gatius, S., Zamora, C., Vidal, S., Salud, A., 2019. Respirology 24, 799–804.
Pothipor, C., Bamrungsap, S., Jakmunee, J., Ounnunkad, K., 2022. Colloids Surf. B Biointerfaces 210, 112260.
Prasad, K.S., Cao, X., Gao, N., Jin, Q., Sanjay, S.T., Henao-Pabon, G., Li, X., 2020. Sensor. Actuator. B Chem. 305, 127516.
Pujol, J.L., Grenier, J., Daures, J.P., Daver, A., Pujol, H., Michel, F.B., 1993. Cancer Res. 53, 61–66.
Rahimzadeh, Z., Naghib, S. M., Askari, E., Molaabasi, F., Sadr, A., Zare, Y., Afsharpad, M., and Rhee, K. Y. (2021) 10, 744-753..
Rajarathinam, T., Kwon, M., Thirumalai, D., Kim, S., Lee, S., Yoon, J.-H., Paik, H.-j., Kim, S., Lee, J., Ha, H.K., Chang, S.-C., 2021. Anal. Chim. Acta 1175, 338749.
Ranjan, P., Abubakar Sadique, M., Yadav, S., Khan, R., 2022. ACS Appl. Mater. Interfaces 14, 20802–20812.
Rifai, N., Gillette, M.A., Carr, S.A., 2006. Nat. Biotechnol. 24, 971–983.
Sadeghi, M., Kashanian, S., Naghib, S. M., Askari, E., Haghiralsadat, F., and Tofighi, D. (2022a) 11, 793-810..
Sadeghi, M., Kashanian, S., Naghib, S.M., Haghiralsadat, F., Tofighi, D., 2022b. Int. J. Electrochem. Sci. 17.
Sadighbayan, D., Sadighbayan, K., Khosroushahi, A.Y., Hasanzadeh, M., 2019a. Trac. Trends Anal. Chem. 119, 1–29.
Sadighbayan, D., Sadighbayan, K., Tohid-Kia, M.R., Khosroushahi, A.Y., Hasanzadeh, M., 2019b. Trac. Trends Anal. Chem. 118, 73–88.
Saeed, A.A., Sanchez, J.L.A., O'Sullivan, C.K., Abbas, M.N., 2017. Bioelectrochemistry 118, 91–99.
Sanchez-Carbayo, M., Espasa, A., Chinchilla, V., Herrero, E., Megias, J., Mira, A., Soria, F., 1999. Clin. Chem. 45, 1944–1953.
Senf, B., Yeo, W.H., Kim, J.H., 2020. Biosens. Bioelectron. 10, 23.
Settu, K., Liu, J.T., Chen, C.J., Tsai, J.Z., 2017. Anal. Biochem. 534, 99–107.
Shang, L., Zhao, X.H., Zhang, W., Jia, L.P., Ma, R.N., Xue, Q.W., Wang, H.S., Guo, A.X., Si, L., 2021. Mikrochim. Acta 189, 17.
Shao, Y.Y., Wang, J., Engelhard, M., Wang, C.M., Lin, Y.H., 2010. J. Mater. Chem. 20, 743–748.
Sharifi, M., Avadi, M.R., Attar, F., Dashtestani, F., Ghorchian, H., Rezayat, S.M., Saboury, A.A., Falahati, M., 2019. Biosens. Bioelectron. 126, 773–784.
Sharifi, M., Hasan, A., Attar, F., Taghizadeh, A., Falahati, M., 2020. Talanta 217, 1–12.
Shrivastava, S.R., Shrivastava, P.S., Ramasamy, J., 2014. Iran. J. Cancer Prev. 7, 58–59.
Siegel, R., Naishadham, D., Jemal, A., 2013. Ca - Cancer J. Clin. 63, 11–30.
Siemer, S., Wunsch, D., Khamis, A., Lu, Q., Scherberich, A., Filippi, M., KraffT, M.P., Hagemann, J., Weiss, C., Ding, G.B., Stauber, R.H., Gribko, A., 2020. Nanomaterials 10, 1–28.
Solanki, S., Gupta, A.K., Saha, U., Krasnoslobodtsev, A.V., Gupta, R.K., Malhotra, B.D., 2023. Sustain. Energy Technol. Assessments 57, 13.
Soldano, C., Mahmood, A., Dujardin, E., 2010. Carbon 48, 2127–2150.
St John, M.A.R., Li, Y., Zhou, X.F., Denny, P., Ho, C.M., Montemagno, C., Shi, W.Y., Qi, F. X., Wu, B., Sinha, U., Jordan, R., Wolinsky, L., Park, N.H., Liu, H.H., Abemayor, E., Wong, D.T.W., 2004. Arch. Otolaryngol. Head Neck Surg. 130, 929–935.
Strnadel, J., Choi, S., Fujimura, K., Wang, H., Zhang, W., Wyse, M., Wright, T., Gross, E., Peinado, C., and Park, H. W. J. C. r. (2017) 77, 1997-2007..
Strobel, C., Forster, M., Hilger, I., 2014. Beilstein J. Nanotechnol. 5, 1795–1807.
Szarvas, T., Becker, M., Vom Dorp, F., Gethmann, C., Tötsch, M., Bánkfalvi, Á., Schmid, K. W., Romics, I., Rübben, H., and Ergün, S. J. C. s. (2010) 101, 1300-1308..
Tan, S.H., Petrovics, G., Srivastava, S., 2018. Int. J. Mol. Sci. 19, 1–31.
Tauro, B.J., Greening, D.W., Mathias, R.A., Ji, H., Mathivanan, S., Scott, A.M., Simpson, R.J., 2012. Methods 56, 293–304.
Teklu, A., Barry, C., Palumbo, M., Weiwadel, C., Kuthirummal, N., Flagg, J., 2019. Adv. Condens. Matter Phys. 2019, 13.
Teles, F., Tavira, L., da Fonseca, L.J.P., 2010. Crit. Rev. Clin. Lab Sci. 47, 139–169.
Thunkhamrak, C., Chuntib, P., Ounnunkad, K., Banet, P., Aubert, P.H., Saianand, G., Gopalan, A.I., Jakmunee, J., 2020. Talanta 208, 1–9.
Tiwari, S., Gupta, P.K., Bagbi, Y., Sarkar, T., Solanki, P.R., 2017. Biosens. Bioelectron. 89, 1042–1052.
Torul, H., Yarali, E., Eksin, E., Ganguly, A., Benson, J., Tamer, U., Papakonstantinou, P., Erdem, A., 2021. Biosensors 11.
Verma, S., Singh, S.P., 2019. MRS Commun 9, 1227–1234.
Verma, M.L., Barrow, C.J., Puri, M., 2013. Appl. Microbiol. Biotechnol. 97, 23–39.
Verma, S., Singh, A., Shukla, A., Kaswan, J., Arora, K., Ramirez-Vick, J., Singh, P., Singh, S.P., 2017. ACS Appl. Mater. Interfaces 9, 27462–27474.
Wang, X., Zhi, L.J., Mullen, K., 2008. Nano Lett. 8, 323–327.
Wang, D., Chai, Y.Q., Yuan, Y.L., Yuan, R., 2017. Anal. Chem. 89, 8951–8956.
Wang, X., Wang, Y.Y., Ye, X.X., Wu, T., Deng, H.P., Wu, P., Li, C.Y., 2018. Biosens. Bioelectron. 99, 34–39.
Wang, Y., Sun, S., Luo, J., Xiong, Y., Ming, T., Liu, J., Ma, Y., Yan, S., Yang, Y., Yang, Z., Reboud, J., Yin, H., Cooper, J.M., Cai, X., 2020. Microsystems & Nanoengineering 6, 32.
Wang, H.Y., Sun, J.J., Lu, L., Yang, X., Xia, J.F., Zhang, F.F., Wang, Z.H., 2020. Anal. Chim. Acta 1094, 18–25.
Wolff, A.C., Hammond, M.E.H., Schwartz, J.N., Hagerty, K.L., Allred, D.C., Cote, R.J., Dowsett, M., Fitzgibbons, P.L., Hanna, W.M., Langer, A., McShane, L.M., Paik, S., Pegram, M.D., Perez, E.A., Press, M.F., Rhodes, A., Sturgeon, C., Taube, S.E., Tubbs, R., Vance, G.H., de Vijver, M.V., Wheeler, T.M., Hayes, D.F., 2007. J. Clin. Oncol. 25, 118–145.
Wu, L.L., Chiou, C.C., Chang, P.Y., Wu, J.T., 2004. Clin. Chim. Acta 339, 1–9.
Wu, Z.S., Ren, W.C., Gao, L.B., Zhao, J.P., Chen, Z.P., Liu, B.L., Tang, D.M., Yu, B., Jiang, C.B., Cheng, H.M., 2009. ACS Nano 3, 411–417.
Wu, L.T., Liu, Y., Chi, B., Xu, Z., Feng, X.H., Li, S., Xu, H., 2015. Food Chem. 187, 182–188.
Xia, T.T., Liu, C.Z., Hu, J.H., Guo, C., 2016. Chem. Eng. J. 295, 201–206.
Xiang, W.W., Lv, Q.X., Shi, H.X., Xie, B., Gao, L., 2020. Talanta 214, 1–17.
Xu, L., Wen, Y., Pandit, S., Mokkapati, V.R.S.S., Mijakovic, I., Li, Y., Ding, M., Ren, S., Li, W., Liu, G., 2019. BMC Chemistry 13, 112.
Yaiwong, P., Semakul, N., Bamrungsap, S., Jakmunee, J., Ounnunkad, K., 2021. Bioelectrochemistry 142, 107944.
Yamamoto, K., Oka, M., Hayashi, H., Tangoku, A., Gondo, T., Suzuki, T., 1997. Cancer 79, 1647–1655.
Yan, Y., Zuo, X., Wei, D., 2015. Stem Cells Translational Medicine 4, 1033–1043.
Yang, W.R., Ratinac, K.R., Ringer, S.P., Thordarson, P., Gooding, J.J., Braet, F., 2010. Angew. Chem.-Int. Edit. 49, 2114–2138.
Yang, K., Wan, J.M., Zhang, S., Tian, B., Zhang, Y.J., Liu, Z., 2012. Biomaterials 33, 2206–2214.
Yang, K., Feng, L.Z., Shi, X.Z., Liu, Z., 2013. Chem. Soc. Rev. 42, 530–547.
Yang, M.Q., Zhang, N., Pagliaro, M., Xu, Y.J., 2014. Chem. Soc. Rev. 43, 8240–8254.
Yang, M.Q., Han, C., Zhang, N., Xu, Y.J., 2015. Nanoscale 7, 18062–18070.
Yang, Y., Zhang, R.Q., Zhou, B.N., Song, J.Y., Su, P., Yang, Y., 2017. ACS Appl. Mater. Interfaces 9, 37254–37263.
Yang, G., Xiao, Z., Tang, C., Deng, Y., Huang, H., He, Z., 2019. Biosens. Bioelectron. 141, 111416.
Yoon, H.J., Kozminsky, M., Nagrath, S., 2014. ACS Nano 8, 1995–2017.
Zhang, L.M., Xia, J.G., Zhao, Q.H., Liu, L.W., Zhang, Z.J., 2010. Small 6, 537–544.
Zhang, L.M., Lu, Z.X., Zhao, Q.H., Huang, J., Shen, H., Zhang, Z.J., 2011. Small 7, 460–464.
Zhang, M., Zhang, X.H., He, X.W., Chen, L.X., Zhang, Y.K., 2012. Nanoscale 4, 3141–3147.
Zhou, S.W., Wang, Y.Y., Zhu, J.J., 2016. ACS Appl. Mater. Interfaces 8, 7674–7682.